

LYMAN α EMITTERS AT REDSHIFT 5.7 IN THE COSMOS FIELD ¹

T. MURAYAMA ², Y. TANIGUCHI ³, N. Z. SCOVILLE ^{4, 5}, M. AJIKI ², D. B. SANDERS ⁵, B. MOBASHER ⁶, H. AUSSEL ^{5, 7}, P. CAPAK ⁴, A. KOEKEMOER ⁶, Y. SHIOYA ³, T. NAGAO ^{8, 9}, C. CARILLI ¹⁰, R. S. ELLIS ⁴, B. GARILLI ¹¹, M. GIAVALISCO ⁶, M. G. KITZBICHLER ¹², O. LEFEVRE ¹³, D. MACCAGNI ¹¹, E. SCHINNERER ¹⁴, V. SMOLCIC ^{15, 16}, S. TRIBIANO ^{17, 18}, A. CIMATTI ⁹, Y. KOMIYAMA ⁸, S. MIYAZAKI ¹⁹, S. S. SASAKI ^{2, 4}, J. KODA ⁴, AND H. KAROJI ⁸

Draft version July 23, 2018

ABSTRACT

We present results from a narrow-band optical survey of a contiguous area of 1.95 deg², covered by the Cosmic Evolution Survey (COSMOS). Both optical narrow-band ($\lambda_c = 8150 \text{ \AA}$ and $\Delta\lambda = 120 \text{ \AA}$) and broad-band (B , V , g' , r' , i' , and z') imaging observations were performed with the Subaru prime-focus camera, Suprime-Cam on the Subaru Telescope. We provide the largest contiguous narrow-band survey, targeting Ly α emitters (LAEs) at $z \approx 5.7$. We find a total of 119 LAE candidates at $z \approx 5.7$. Over the wide-area covered by this survey, we find no strong evidence for large scale clustering of LAEs. We estimate a star formation rate (SFR) density of $\sim 7 \times 10^{-4} M_{\odot} \text{ yr}^{-1} \text{ Mpc}^{-3}$ for LAEs at $z \approx 5.7$, and compare it with previous measurements.

Subject headings: cosmology: observations — cosmology: early universe — galaxies: formation — galaxies: evolution

1. INTRODUCTION

Understanding of the formation and early evolution of galaxies requires study of rest-frame properties of well-defined samples of high-redshift galaxies. These are needed to address the cosmic star formation history and growth of large scale structures in the early Universe and the source of cosmic reionization of intergalactic space. There are two widely used techniques to select such high-redshift galaxies: (1) Lyman Break technique, aiming for Lyman Break Galaxies (LBGs; Steidel et al. 1999; Iwata

et al. 2003; Ouchi et al. 2004; Bouwens & Illingworth 2006 and references therein), and (2) narrow-band imaging surveys, targeting Ly α emitters (LAEs; Hu & McMahon 1996; Rhoads & Malhotra 2001; Ajiki et al. 2003; Hu et al. 2004; Taniguchi et al. 2005 and references therein). The narrow-band surveys are mainly aimed at star-forming population while Lyman Break technique also selects galaxies with older age.

Recently, LAE surveys have extended study of the clustering and morphology of star-forming galaxies to the highest redshifts (Shimasaku et al. 2004; Ouchi et al. 2005; Ajiki et al. 2006; Mobasher et al. 2006). Indeed, some of the previous LAE surveys have shown signs of large scale structures, either using 2-D projected distribution of galaxies or 3-D distribution, also using redshifts. For example, evidence for clustering of LAEs at $z \approx 4.9$ was found over an area of $\simeq 0.5$ degree \times 0.5 degree, covered by the Subaru Deep Field (SDF) (Shimasaku et al. 2004; see also Ouchi et al. 2003), extending to ~ 20 Mpc \times 50 Mpc. However, no such structures were found for LAEs at $z \approx 5.7$ (Shimasaku et al. 2006) and $z \approx 6.6$ (Taniguchi et al. 2005; Kashikawa et al. 2006). Although, using a spectroscopically confirmed sample of 34 LAEs at $z \approx 5.7$, Shimasaku et al. (2006) found evidence for weak clustering. In an independent study, using a spectroscopically confirmed sample of 19 LAEs at $z \approx 5.7$, Hu et al. (2004) found structures extending to angular scales of ~ 60 Mpc with evidence for filamentary structures. This result was further confirmed by Ouchi et al. (2005) who found filamentary structures of size 10 – 40 Mpc in the Subaru XMM-Newton Deep Survey (SXDS; Sekiguchi et al. 2004), using a photometric sample of 515 LAEs. In addition to the above results, based on deep narrow-band surveys in so-called “blank fields”, evidence has been accumulating in support of clustering at $z = 4.1$ to 5.2, with a few Mpc scales around high-redshift radio galaxies (Venemans et al. 2002, 2004; Overzier et al. 2006) and quasar SDSS J0836+0054 (Zheng et al. 2006; Ajiki et al. 2006b).

These studies are useful in investigating early forma-

¹ Based on data collected at the Subaru Telescope, which is operated by the National Astronomical Observatory of Japan

² Astronomical Institute, Graduate School of Science, Tohoku University, Aramaki, Aoba, Sendai 980-8578, Japan

³ Physics Department, Graduate School of Science & Engineering, Ehime University, 2-5 Bunkyo-cho, Matsuyama 790-8577, Japan

⁴ Department of Astronomy, MS 105-24, California Institute of Technology, Pasadena, CA 91125

⁵ Institute for Astronomy, University of Hawaii, 2680 Woodlawn Drive, HI 96822

⁶ Space Telescope Science Institute, 3700 San Martin Drive, Baltimore, MD 21218

⁷ CEA Saclay, DSM/DAPNIA/Sap, 91191 Gif-sur-Yvette Cedex, France

⁸ National Astronomical Observatory of Japan, 2-21-1, Osawa, Mitaka, Tokyo 181-8588, Japan

⁹ INAF — Osservatorio Astrofisico di Arcetri, Largo Enrico Fermi 5, 50125 Firenze, Italy

¹⁰ National Radio Astronomy Observatory, P.O. Box 0, Socorro, NM 87801-0387

¹¹ INAF, Istituto di Astrofisica Spaziale e Fisica Cosmica, Sezione di Milano, via Bassini 15, 20133 Milano

¹² Max-Planck-Institut für Astrophysik, D-85748 Garching bei München, Germany

¹³ Laboratoire d’Astrophysique de Marseille, BP 8, Traverse du Siphon, 13376 Marseille Cedex 12, France

¹⁴ Max Planck Institut für Astronomie, Königstuhl 17, Heidelberg, D-69117, Germany

¹⁵ Princeton University Observatory, Princeton, NJ 08544

¹⁶ University of Zagreb, Department of Physics, Bijenicka cesta 32, 10000 Zagreb, Croatia

¹⁷ American Museum of Natural History

¹⁸ CUNY Bronx Community College, New York, NY

¹⁹ Subaru Telescope, National Astronomical Observatory of Japan, 650 N. A’ohoku Place, Hilo, HI 96720

tion of galaxies and large-scale structures. Furthermore, they provide important constraints on both the star formation and cosmic re-ionization history. A detailed study of clustering of galaxies at high-redshifts requires deep and wide-area surveys to allow a homogeneously selected sample of galaxies and to minimise effects of cosmic variance. This is the subject of the present paper.

In this paper we present the largest survey of LAEs at $z \approx 5.7$, covering the entire 2 square degree field of the Cosmic Evolution Survey (COSMOS), centered at $\alpha(\text{J2000.0}) = 10^{\text{h}} 00^{\text{m}} 28.6^{\text{s}}$ and $\delta(\text{J2000.0}) = +02^{\circ} 12' 21.0''$ (Scoville et al. 2007). The full COSMOS field has been observed in I_{814} -band with the Advanced Camera for Surveys (ACS) on-board the Hubble Space Telescope (HST). In addition to the ACS data, the multi-wavelength broad and narrow-band observations were also performed using the Suprime-Cam (Miyazaki et al. 2002) on the Subaru Telescope (Kaifu et al. 2000; Iye et al. 2004). The narrow-band filter *NB816* has an effective wavelength of $\lambda_c = 8150 \text{ \AA}$ with a width $\Delta\lambda = 120 \text{ \AA}$ (see Ajiki et al. 2003 for details), allowing to select LAEs in the range $5.65 < z < 5.75$. We assume standard cosmology with $\Omega_{\text{matter}} = 0.3$, $\Omega_{\Lambda} = 0.7$, and $H_0 = 70 \text{ km s}^{-1} \text{ Mpc}^{-1}$. Throughout this paper, we use magnitudes in the AB system.

2. OBSERVATIONS AND SAMPLE SELECTION

2.1. Data and Source Detection

We carried out an optical narrow-band (*NB816*) imaging survey of the entire 2-deg² area of the COSMOS field, using the Suprime-Cam on the Subaru Telescope. These observations, combined with the broad-band (B , V , g' , r' , i' , and z') Suprime-Cam and ACS (I_{814}) photometric data will be used to identify LAE candidates at $z \sim 5.7$ and to study their properties. Details of the narrow-band and ground-based observations and data reduction are given in Taniguchi et al. (2007) and Capak et al. (2007a) and for the HST-ACS observations in Koekemoer et al. (2007).

For the ground-based observations, the seeing size varies between the exposures. The PSF size of each *NB816* images is between $0''.4$ and $0''.7$. To optimize source detection in *NB816*, we only use exposures with PSF sizes smaller than $1''.15$ to construct a combined image.

The limiting magnitude of the *NB816* has a variance of ~ 0.5 mag, depending on the location on the image. We only confine our LAE search to areas with low noise where the 5σ limiting magnitude with a $2''$ diameter aperture in *NB816* is ~ 25.1 . This corresponds to a total effective area of 1.95 deg^2 . The transverse co-moving area of the LAE survey at $z = 5.7$ is $3.9 \times 10^4 \text{ Mpc}^2$. The FWHM of the filter, which has a Gaussian-like shape, corresponds to a co-moving depth of 45 Mpc, spanning the redshift range $5.65 < z < 5.75$ along the line-of-sight. Therefore, our *NB816* survey probes a volume of $1.8 \times 10^6 \text{ Mpc}^3$.

We have performed source detection and photometry on the *NB816* image with SExtractor version 2.3 (Bertin & Arnouts 1996). A source is selected as a contiguous 9-pixel area above the 3σ noise level (corresponding to $26.48 \text{ mag arcsec}^{-2}$) on the *NB816* image. Photometry is performed on the *NB816* and the broadband images over

$0''.5$, $2''$, and $3''$ diameter apertures. To the magnitude limit of the survey [*NB816*($2''\phi$) = 25.1], we find $\sim 3 \times 10^5$ sources.

2.2. Selection of LAE Candidates

Our main aim in the present survey is to identify reliable LAE candidates at $z \approx 5.7$ by first selecting *NB816* excess objects, using the following criteria:

$$NB816(2''\phi) < 25.1, \quad (1)$$

$$iz(2''\phi) - NB816(2''\phi) > \max(0.7, 3\sigma_{iz-NB816}), \quad (2)$$

$$B(0''.5\phi) > 29.6, \quad (3)$$

$$g'(0''.5\phi) > 29.2, \quad (4)$$

$$V(0''.5\phi) > 29.1, \text{ and} \quad (5)$$

$$r'(0''.5\phi) > 29.1, \quad (6)$$

where iz is the continuum magnitude at $\lambda = 8150 \text{ \AA}$, estimated by linear interpolation between i' and z' flux densities ($f_{iz} = 0.57f_{i'} + 0.43f_{z'}$). The first criterion ensures that objects are detected above the 5σ level in the *NB816*. The criterion 2 allows selection of emission-line objects with observed equivalent width, $EW_{\text{obs}} \geq 120 \text{ \AA}$. The 3σ of $iz - NB816$ is estimated from the local-background noise measurement of the most noisy region in the survey area. This is illustrated in Figure 1 where the LAE candidates are identified on $iz - NB816$ vs. *NB816* color—magnitude diagram. The criteria (3), (4), (5), and (6) ensure that $z \approx 5.7$ candidates are undetected (at $\approx 1.5\sigma$ noise level) in B , g' , V , and r' bands. We adopt magnitudes in a $0''.5$ diameter aperture to avoid possible contamination by low- z foreground objects.

We find a total of 119 LAE candidates at $z \sim 5.7$ that satisfy the above criteria and confirm these by careful eye inspection for apparent false detections. Our first spectroscopic followup observation of ~ 50 LAE candidates indicates a $\sim 95\%$ or better confirmation rate (Capak et al. 2007b). We also find that there is no low-luminosity radio-loud AGN with $L(1.4\text{GHz}) > 6 \times 10^{24} \text{ W Hz}^{-1}$ among our final LAE candidates (Carilli et al. 2007). The coordinates and photometric data for the LAE candidates are listed in Table 1. All magnitudes are corrected for Galactic extinction; $E(B - V) = 0.0195$ (Capak et al. 2007a). In Table 1 we also list emission line fluxes and observed equivalent widths estimated from *NB816* and z' flux densities in a $3''$ aperture.

As shown by the criterion 2, the detection limit of LAEs depends on the depth of both the *NB816* and i' and z' band images. However, we did not impose any noise threshold on the i' and z' band images when we selected the LAE candidates. To ensure homogeneity, we make a subsample of the LAE candidates in areas with low noise, both in the i' and z' bands where the 5σ limiting magnitude over a $2''$ diameter aperture is brighter than 25.4 or 24.8 mag in i' and z' bands respectively. This subsample (hereafter, the statistical sample) contains 111 LAE candidates which are identified by asterisks in Table 1. We use this “statistical sample” to estimate statistical properties of LAEs, including their number density and luminosity function. The size of the effective area corresponding to this statistical sample is reduced to 1.86 deg^2 , equivalent to $3.7 \times 10^4 \text{ Mpc}^2$ of the

transverse co-moving area at $z=5.7$. The survey volume for the statistical sample is $1.7 \times 10^6 \text{ Mpc}^3$.

3. RESULTS AND DISCUSSION

3.1. Spatial Distribution and Angular Two-Point Correlation Function

In Figure 3, we show the spatial distribution of all the LAE candidates in our sample. There appears to be little evidence for strong clustering. When dividing the survey area into four tiles with $0.7 \text{ degree} \times 0.7 \text{ degree}$ each, we find 26, 28, 26, and 31 LAEs in the SW, NW, SE, and NE quadrant respectively. Therefore, the 111 LAE candidates in the statistical sample are almost randomly distributed at least in large scale.

We derive the angular two-point correlation function (ACF), $w(\theta)$, for the 111 LAE candidates in the “statistical sample” using the estimator defined by Landy & Szalay (1993)

$$w(\theta) = \frac{DD(\theta) - 2DR(\theta) + RR(\theta)}{RR(\theta)}, \quad (7)$$

where $DD(\theta)$, $DR(\theta)$, and $RR(\theta)$ are normalized numbers of galaxy-galaxy, galaxy-random, and random-random pairs, respectively. The random sample consists of 100,000 sources with the same geometrical constraints as the LAE sample.

In the left panel of Figure 4, we show the ACF for the statistical LAE sample (large filled circles). There is a clustering signal with 2.8σ significance at 25 arcsec ($\simeq 1.0 \text{ Mpc}$ at $z = 5.7$). We also find possible signals at 63 arcsec , 100 arcsec , 158 arcsec , and 251 arcsec although their detection significance is as low as $\simeq 1.3\sigma$. We compare this with the ACF for LAE candidates at $z \approx 5.7$ in the SDF (Shimasaku et al. 2006) using their whole sample; $NB816 \leq 26.5$ (small filled circles) and their bright sample; $NB816 \leq 25.5$ (open circles). Most of data points are consistent within 1σ errors among the three samples. However, there seems to be possible difference among the three samples at small angular scales. Since our LAE sample is limited at $NB816 < 25.1$, the brighter sample seems to show the larger $w(\theta)$ at $\theta \leq 30 \text{ arcsec}$.

Although the clustering signals are not high, particularly at larger scales (e.g., $\theta \geq 100 \text{ arcsec}$), the LAE candidates in the COSMOS field follow a power-law relation between $w(\theta)$ and θ , as shown in the right panel (i.e. $w(\theta) = A_w \theta^\beta$). We find a best fit power law with an index of $\beta = -1.2 \pm 0.2$ and an amplitude at 1 arcsec of $A_w = 95 \pm 76$. For this power law fit, we only used data points between 25 arcsec and 1585 arcsec except the point at 398 arcsec . The value of β is steeper than $\beta = -0.74$ (at $z = 4$) and $\beta = -0.81$ (at $z = 5$) found for Lyman break galaxies in the SDF (Kashikawa et al. 2006). The semi-analytic models predict that the ACF for higher halo mass has a steeper slope and a stronger amplitude (Kashikawa et al. 2006), our results imply that the LAEs are embedded in massive dark matter halo, e.g., heavier than $10^{12} M_\odot$ (Ouchi et al. 2004). However, absence of significant clustering signal for LAEs at $z \approx 5.7$ in the SDF (Shimasaku et al. (2006)) may be indicative of cosmic variance in these studies.

3.2. Ly α Luminosities of LAE Candidates

Using our total sample of LAE candidates at $z \approx 5.7$ and a volume of $1.7 \times 10^6 \text{ Mpc}^3$, we estimate a space density of $n(\text{Ly}\alpha) \approx 6.6 \times 10^{-5} \text{ Mpc}^{-3}$ for the LAE candidates in our “statistical sample”. This is a factor of 1.6 lower than those in previous LAE surveys with nearly the same $NB816$ limits ($NB816 \approx 25$) (Ajiki et al. 2003; Hu et al. 2004). The observed difference is likely caused by cosmic variance.

We measure the Ly α luminosity, $L(\text{Ly}\alpha)$, of our LAE candidates, assuming all the LAEs to be at $z = 5.70$. The rest-frame equivalent widths and Ly α luminosities as listed in Table 1. We adopted aperture magnitudes measured over a $3''$ aperture diameter for estimation of the Ly α luminosity. We find that the magnitudes measured over $2''$ and $3''$ apertures are well correlated with a small systematic offset. However, the total magnitudes from SExtractor (MAGAUTO) show large scatter when compared with the aperture magnitudes measured over $2''$ and $3''$ diameter apertures due to contamination by neighboring objects. The derived Ly α luminosities range from $\approx 6.3 \times 10^{42} \text{ ergs s}^{-1}$ to $\approx 3.1 \times 10^{43} \text{ ergs s}^{-1}$.

Using the 111 LAE candidates in our “statistical sample”, we constructed the Ly α luminosity function, as shown in the left panel of Figure 5. We compare this with other Ly α luminosity functions at $z \sim 5.7$ (Rhoads & Malhotra 2001; Ajiki et al. 2003, 2006a; Hu et al. 2004). Our survey has a luminosity limit of $L_{\text{lim}}(\text{Ly}\alpha) = 6.3 \times 10^{42} \text{ ergs s}^{-1}$, corresponding to a LAE with $NB816 = 25.1$, undetected in i' and in z' . This limit is similar to those in Ajiki et al. (2003) and Hu et al. (2004). The luminosity functions do not show any significant difference at the luminous part [$L(\text{Ly}\alpha) \geq 10^{43} \text{ ergs s}^{-1}$], although the number density of Rhoads & Malhotra (2001) is smaller compared to those in other surveys. Because of the improved Poisson statistics in the COSMOS LAE sample, the errorbars in this survey are relatively smaller. Therefore, the brighter part of the LAE luminosity function is relatively well established. Also, the wide area covered by the COSMOS survey enables us to improve the statistics at the brighter part of the luminosity function ($L(\text{Ly}\alpha) > 2 \times 10^{43} \text{ ergs s}^{-1}$) by increasing the number of luminous LAEs per luminosity bin compared to previous surveys. At $10^{42.8} \leq L(\text{Ly}\alpha) < 10^{43.0} \text{ ergs s}^{-1}$, the number density from this study is almost the same as that of Rhoads & Malhotra (2001) and Ajiki et al. (2006a) while is smaller (by a factor of 2) than that estimated in Hu et al. (2004) and Ajiki et al. (2003). This is, at least partly, due to both spatial variance and incompleteness at $10^{42.8} \leq L(\text{Ly}\alpha) < 10^{43.0} \text{ ergs s}^{-1}$ in our survey.

In Figure 5 (right panel), we also compare our result with those of previous LAE surveys as a function of redshift. The LAE luminosity functions at $z = 3.4$, $z = 4.9$, and $z = 6.6$ are taken from Cowie & Hu (1998), Ouchi et al. (2003), and Taniguchi et al. (2005), respectively. COSMOS ($z = 5.7$) and Taniguchi et al. 2005 ($z = 6.6$) give almost the same result within errors at the bright end ($L(\text{Ly}\alpha) \geq 10^{43} \text{ ergs s}^{-1}$). No LAE with $L(\text{Ly}\alpha) \geq 10^{43} \text{ ergs s}^{-1}$ is found in the previous LAE surveys at $z = 3.4$ and $z = 4.9$. While there are differences on the detection completeness and the contamination rates among the surveys, this may provide evidence for the number and/or luminosity evolutions of LAEs.

3.3. Star Formation Rates

We now estimate the contribution from LAEs to the star formation rate (SFR) at $z \approx 5.7$, using the following relation (Kennicutt 1998; Brocklehurst 1971),

$$SFR(\text{Ly}\alpha) = 9.1 \times 10^{-43} L(\text{Ly}\alpha) M_{\odot} \text{ yr}^{-1}, \quad (8)$$

where $L(\text{Ly}\alpha)$ is in ergs s^{-1} . We assume Salpeter initial mass function with $(m_{\text{lower}}, m_{\text{upper}}) = (0.1 M_{\odot}, 100 M_{\odot})$.

The estimated SFRs are given in the forth column of Table 1. They range from 5.7 to 28.3 $M_{\odot} \text{ yr}^{-1}$ with a median value of 9.6 $M_{\odot} \text{ yr}^{-1}$. The SFRs derived here can be underestimated due to the effect of absorption by H I gas both in the host galaxies and in the intergalactic medium and dusts in the host galaxies. SFRs independent of the absorption are estimated by the radio data; an upper limit to the mean massive star formation rate (5 M_{\odot} to 100 M_{\odot}) for the LAE sample is derived as $\sim 100 M_{\odot} \text{ yr}^{-1}$ (Carilli et al. 2007).

The estimated SFRs from the Ly α luminosities here are comparable to those of LAEs at $z \simeq 5.7 - 6.6$ (e.g., Ajiki et al. 2003; Taniguchi et al. 2005). The SFR density at $z = 5.7$ is estimated by summing up the Ly α luminosities of the 111 “statistical candidates” and corresponds to $7.2 \times 10^{-4} M_{\odot} \text{ yr}^{-1} \text{ Mpc}^{-3}$, similar to those obtained in previous narrow-band surveys.

It would be instructive to examine whether the SFRs derived from the Ly α luminosity here are consistent with those based on the UV continuum luminosity from the broad-band data. The observed z' magnitudes, measured over $3''$ aperture diameters, are converted to UV continuum luminosities at $\lambda = 1270 \text{ \AA}$ and used to estimate the SFRs, using the relation (Kennicutt 1998; see also Madau et al. 1998),

$$SFR(\text{UV}) = 1.4 \times 10^{-28} L_{\nu} M_{\odot} \text{ yr}^{-1}, \quad (9)$$

where L_{ν} is the UV continuum luminosity in $\text{ergs s}^{-1} \text{ Hz}^{-1}$. For each object, we estimate the SFR from its rest-frame UV ($\lambda = 1270 \text{ \AA}$) continuum luminosity, with the results summarized in Table 1. Comparison between $SFR(\text{Ly}\alpha)$ and $SFR(\text{UV})$ in Figure 6 shows that, on average, $SFR(\text{UV})$ is relatively higher than $SFR(\text{Ly}\alpha)$ for most of the LAE candidates. We find an average ratio of $SFR_{\text{total}}(\text{Ly}\alpha) / SFR_{\text{total}}(\text{UV}) = 0.68$, where $SFR_{\text{total}}(\text{Ly}\alpha)$ and $SFR_{\text{total}}(\text{UV})$ are, respectively, the sum of SFRs of all our 119 LAE candidates from Ly α

line and UV continuum. The relatively lower $SFR(\text{Ly}\alpha)$ compared to $SFR(\text{UV})$ is likely due to the effect of the differential absorption. However, some of our LAE candidates have $SFR(\text{Ly}\alpha)/SFR(\text{UV}) > 1$, e.g., those ratios of #13, #27, #50, #71, and #114 are greater than unity with 2σ significance. They may be in a very early phase ($< 10^8 \text{ yr}$) of star formation activity in which $SFR(\text{UV})$ is underestimated (Schaerer 2000; see also Nagao et al. 2004, 2005).

4. SUMMARY

We have presented results from our narrow-band deep imaging survey of the COSMOS field, targetting LAEs at $z \approx 5.7$. This is the largest contiguous survey of LAEs. Our main results are summarized below:

(1) We found 119 LAE candidates in our narrow-band survey. Allowing for changes in the noise level over the entire field, we extracted a subsample of 111 LAEs that is used to make our statistical analysis.

(2) We find no significant evidence for clustering of LAEs at $z \sim 5.7$ contrary to some of the previous LAE surveys.

(3) An analysis of angular two-point correlation function gives the power-law relation $w(\theta) = A_w \theta^{\beta}$, with $\beta = -1.2 \pm 0.2$. The power-law index here is steeper than that found for Lyman break galaxies at $z = 4$ and 5. This suggests that LAEs at $z \approx 5.7$ might be located in massive dark matter halos with mass of $> 10^{12} M_{\odot}$.

(4) The number density of LAEs and the average star formation rate are similar to those measured in previous surveys. We estimate a star formation rate density of $\sim 7 \times 10^{-4} M_{\odot} \text{ yr}^{-1} \text{ Mpc}^{-3}$ at $z \approx 5.7$.

(5) We measure the Ly α luminosity function at $z > 5$ and extend this to $L(\text{Ly}\alpha) \geq 10^{43} \text{ ergs s}^{-1}$, not explored by previous LAE surveys. We compare the estimated Ly α luminosity function here with those in previous studies in the range $z = 3.4 - 6.6$.

We would like to thank both the Subaru and HST staff for their invaluable help. We also thank Masami Ouchi for providing us his data. This work was financially supported in part by the Ministry of Education, Culture, Sports, Science, and Technology (Nos. 10044052 and 10304013), and by JSPS (15340059 and 17253001). SSS and TN are JSPS fellows.

REFERENCES

- Ajiki, M., et al. 2003, AJ, 126, 2091
 Ajiki, M., Mobasher, B., Taniguchi, Y., Shioya, Y., Nagao, T., Murayama, T., & Sasaki, S. S., 2006a, ApJ, 638, 596
 Ajiki, M., et al. 2006b, PASJ, 58, 499
 Bertin, E., & Arnouts, S. 1996, A&AS, 117, 393
 Bouwens, R. J., & Illingworth, G. D. 1996, Nature, 443, 189
 Brocklehurst, M. 1971, MNRAS, 153, 471
 Capak, P., et al. 2007a, ApJ, submitted
 Capak, P., et al. 2007b, in preparation
 Carilli, C. L., et al. 2007, ApJ, submitted
 Cowie, L. L., & Hu, E. M. 1998, AJ, 115, 1319
 Hu, E. M., Cowie, L. L., Capak, P., McMahon, R. G., Hayashino, T., & Komiyama, Y. 2004, AJ, 127, 563
 Hu, E. M., & McMahon, R. G. 1996, Nature, 382, 281
 Iwata, I., Ohta, K., Tamura, N., Ando, M., Wada, S., Watanabe, C., Akiyama, M., & Aoki, K. 2003, PASJ, 55, 415
 Iye, M., et al. 2004, PASJ, 56, 381
 Kaifu, N., et al. 2000, PASJ, 52, 1
 Kashikawa, N., et al. 2006, ApJ, 637, 631
 Kennicutt, R. C., Jr. 1998, ARA&A, 36, 189
 Koekemoer, A. et al. 2007, ApJ, submitted
 Landy, S., & Szalay, A. S. 1993, ApJ, 412, 64
 Madau, P., Pozzetti, L., & Dickinson, M. 1998, ApJ, 498, 106
 Miyazaki, S. et al. 2002, PASJ, 54, 833
 Nagao, T., et al. 2004, ApJ, 613, L9
 Nagao, T., et al. 2005, ApJ, 634, 142
 Ouchi, M., et al. 2003, ApJ, 582, 60
 Ouchi, M., et al. 2004, ApJ, 611, 685
 Ouchi, M., et al. 2005, ApJ, 620, L1
 Overzier, R. A. et al. 2006, ApJ, 637, 58
 Rhoads, J. E., & Malhotra, S. 2001, ApJ, 563, L5
 Schaerer, D. 2000, in Building the Galaxies: From the Primordial Universe to the Present, eds. F. Hammer, et al. (Gif-sur-Yvette: Editions Frontières), 389

- Scoville, N. Z., et al. 2007, ApJ, submitted
Sekiguchi, K., et al. 2004, ApSS Library, 301, 169
Shimasaku, K., et al. 2004, ApJ, 605, L93
Shimasaku, K., et al. 2006, PASJ, 58, 313
Steidel, C. C., Adelberger, K. L., Giavalisco, M., Dickinson, M., & Pettini, M. 1999, ApJ, 519, 1
Taniguchi, Y., et al. 2005, PASJ, 57, 165
Taniguchi, Y., et al. 2007, ApJ, submitted
Venemans, B. P., et al. 2002, ApJ, 569, L11
Venemans, B. P., et al. 2004, A&A, 424, L17
Zheng, W., et al. 2006, ApJ, 640, 574

TABLE 1 — *Continued*

No. ^a	α (J2000) ($^{\circ}$)	δ (J2000) ($^{\circ}$)	$NB816^b$ ($\phi 2''0$)	i'^b ($\phi 2''0$)	z'^b ($\phi 2''0$)	iz^b ($\phi 2''0$)	$NB816^b$ ($\phi 3''0$)	z'^b ($\phi 3''0$)	$f_{\nu}(NB816)^c$ ($\phi 3''0$)	$f_{\nu}(z')^c$ ($\phi 3''0$)	f_{line}^d	EW_{obs}^e (\AA)
74*	150.3400	+2.8002	24.9	26.6	26.0	26.3	24.4	25.6	6.2 ± 0.7	2.1 ± 1.0	2.8 ± 0.5	294 ± 153
75*	150.3493	+1.9334	24.4	26.7	26.2	26.4	24.2	26.0	7.7 ± 0.7	1.4 ± 1.0	3.8 ± 0.5	602 ± 442
76*	150.3621	+1.7417	24.3	28.0	25.9	26.6	24.0	25.6	8.8 ± 0.6	2.2 ± 0.9	4.2 ± 0.4	427 ± 183
77*	150.3657	+2.5017	24.7	26.8	26.2	26.5	24.3	25.6	7.0 ± 0.7	2.0 ± 1.0	3.2 ± 0.5	355 ± 184
78*	150.3712	+1.8250	23.9	26.1	25.4	25.8	23.5	25.0	14.2 ± 0.6	3.5 ± 0.9	6.7 ± 0.4	427 ± 115
79*	150.3795	+2.5183	24.6	27.1	26.7	26.9	24.4	26.1	6.5 ± 0.8	1.3 ± 1.0	3.2 ± 0.5	530 ± 427
80*	150.3978	+2.7734	24.8	26.5	26.4	26.4	24.3	25.5	6.6 ± 0.7	2.2 ± 1.0	3.0 ± 0.5	296 ± 138
81*	150.4005	+1.8018	24.9	25.9	25.8	25.9	24.6	26.4	5.1 ± 0.7	< 1.1	2.5 ± 0.5	> 510
82*	150.4078	+2.9117	24.8	26.4	25.8	26.1	24.6	25.4	5.2 ± 0.7	2.4 ± 1.1	2.2 ± 0.5	200 ± 104
83*	150.4079	+2.1133	25.0	26.5	25.9	26.2	24.7	25.6	4.8 ± 0.7	2.1 ± 0.9	2.0 ± 0.4	210 ± 103
84*	150.4091	+2.8063	24.1	25.3	24.5	24.9	23.5	24.0	13.9 ± 0.6	9.0 ± 1.0	5.1 ± 0.4	126 ± 17
85*	150.4274	+2.4974	24.1	25.8	25.0	25.4	23.8	24.5	11.5 ± 0.8	5.8 ± 1.0	4.6 ± 0.5	178 ± 37
86*	150.4339	+2.4867	25.0	27.1	27.0	27.0	24.8	26.3	4.6 ± 0.7	1.1 ± 1.1	2.2 ± 0.5	429 ± 419
87*	150.4393	+2.7860	25.1	26.7	26.5	26.6	24.7	25.9	4.8 ± 0.7	1.6 ± 1.0	2.2 ± 0.4	306 ± 199
88*	150.4444	+1.8076	24.7	27.5	99.0	99.0	24.5	99.0	5.6 ± 0.7	< 1.0	3.2 ± 0.5	> 704
89*	150.4685	+2.7071	25.0	28.1	99.0	99.0	24.5	29.6	5.7 ± 0.7	< 1.1	3.1 ± 0.5	> 619
90*	150.4766	+1.5314	25.0	26.7	99.0	99.0	24.7	99.0	4.7 ± 0.7	< 1.1	2.5 ± 0.5	> 523
91*	150.4890	+1.6883	25.1	26.3	28.0	26.8	24.6	29.7	5.2 ± 0.7	< 1.0	2.8 ± 0.5	> 595
92*	150.4984	+2.8138	25.0	27.5	99.0	99.0	24.7	99.0	5.0 ± 0.8	< 1.1	2.7 ± 0.5	> 564
93*	150.5114	+2.7640	25.0	27.4	99.0	99.0	24.9	99.0	4.1 ± 0.7	< 1.1	2.5 ± 0.5	> 532
94*	150.5131	+1.6066	25.0	26.6	28.2	27.1	24.8	27.1	4.4 ± 0.7	< 1.2	2.3 ± 0.5	> 431
95*	150.5362	+2.0874	24.9	27.0	27.2	27.1	24.7	26.9	4.8 ± 0.7	< 1.0	2.4 ± 0.5	> 532
96*	150.5367	+1.9125	24.5	26.5	26.1	26.3	24.1	25.5	8.2 ± 0.7	2.2 ± 1.0	3.8 ± 0.5	378 ± 167
97*	150.5543	+2.8230	24.7	26.8	26.1	26.4	24.4	25.6	6.4 ± 0.7	2.1 ± 1.0	2.9 ± 0.5	308 ± 153
98*	150.5677	+2.5774	24.2	26.2	25.5	25.9	24.0	25.5	8.9 ± 0.7	2.4 ± 1.0	4.2 ± 0.5	388 ± 175
99*	150.5711	+2.3625	24.9	26.1	26.3	26.2	24.6	26.1	5.2 ± 0.6	1.3 ± 1.0	2.5 ± 0.4	429 ± 339
100*	150.5773	+1.6153	25.1	27.3	27.5	27.4	24.8	26.3	4.2 ± 0.7	1.1 ± 1.1	2.0 ± 0.5	392 ± 389
101*	150.6079	+2.4935	25.0	28.2	99.0	99.0	24.8	99.0	4.4 ± 0.7	< 1.0	2.9 ± 0.5	> 656
102*	150.6386	+2.3956	25.1	27.1	26.7	26.9	24.7	26.0	4.6 ± 0.7	1.4 ± 1.1	2.1 ± 0.5	337 ± 273
103	150.6596	+2.6453	24.7	27.5	26.6	27.1	24.4	26.1	6.5 ± 0.7	1.3 ± 0.9	3.2 ± 0.5	553 ± 420
104	150.6806	+2.7643	23.9	26.1	26.7	26.3	23.7	26.2	12.3 ± 0.7	1.2 ± 0.9	6.3 ± 0.5	1140 ± 860
105*	150.6927	+1.8712	25.1	99.0	99.0	99.0	25.1	99.0	3.4 ± 0.7	< 1.0	1.8 ± 0.5	> 398
106*	150.7034	+2.7397	25.0	27.5	99.0	99.0	24.7	99.0	4.9 ± 0.7	< 1.0	2.9 ± 0.5	> 670
107*	150.7111	+2.2247	24.8	27.0	27.2	27.1	24.6	27.7	5.4 ± 0.6	< 1.0	2.8 ± 0.4	> 614
108*	150.7150	+2.2342	24.4	26.8	26.8	26.8	24.2	26.1	7.7 ± 0.6	1.3 ± 1.0	3.8 ± 0.4	623 ± 460
109*	150.7475	+2.8532	24.6	26.8	25.8	26.2	24.3	25.3	7.1 ± 0.9	2.8 ± 1.2	3.1 ± 0.6	246 ± 113
110*	150.7548	+2.0434	24.6	26.6	25.1	25.7	24.3	24.7	6.7 ± 0.8	4.8 ± 1.0	2.4 ± 0.5	110 ± 34
111*	150.7576	+1.8365	24.4	25.8	25.1	25.4	23.9	24.3	10.1 ± 0.8	7.0 ± 1.2	3.6 ± 0.5	114 ± 25
112*	150.7722	+1.8614	25.1	27.3	26.5	26.9	24.6	26.0	5.3 ± 0.7	1.4 ± 1.1	2.5 ± 0.5	396 ± 325
113*	150.7747	+2.1644	24.9	26.1	99.0	99.0	24.6	99.0	5.4 ± 0.7	< 1.1	3.0 ± 0.5	> 617
114*	150.7756	+1.7953	24.3	27.0	99.0	99.0	24.0	99.0	9.5 ± 0.7	< 1.1	5.1 ± 0.5	> 1040
115*	150.7863	+2.6448	23.7	25.4	25.2	25.3	23.4	24.6	16.2 ± 0.8	5.4 ± 1.0	7.3 ± 0.5	304 ± 58
116*	150.7906	+2.2222	25.0	26.8	26.2	26.5	24.7	25.4	4.6 ± 0.7	2.6 ± 1.0	1.8 ± 0.5	151 ± 71
117	150.8054	+2.9250	24.5	25.8	25.1	25.4	24.1	24.8	8.1 ± 1.0	4.3 ± 1.5	3.2 ± 0.7	165 ± 65
118*	150.8211	+2.2498	24.0	26.0	25.8	25.9	23.6	25.5	13.0 ± 0.7	2.3 ± 1.1	6.4 ± 0.5	631 ± 304
119	150.8342	+2.3398	25.0	27.0	26.4	26.7	24.5	25.2	5.8 ± 0.8	3.1 ± 1.3	2.3 ± 0.6	164 ± 79

^a Asterisks denote the statistical sample.

^b AB magnitude. An entry of “99.0” indicates that no excess flux was measured. All of our LAE candidates are undetected in the B -, g' -, V -, r' -band data.

^c Flux densities of the $NB816$ band and the z' band in unit of $10^{-30} \text{ erg s}^{-1} \text{ cm}^{-2} \text{ Hz}^{-1}$. Errors and upper-limits represent 1σ significance.

^d Estimated line fluxes in unit of $10^{-17} \text{ erg s}^{-1} \text{ cm}^{-2}$. Errors represent 1σ significance.

^e Estimated observed equivalent widths. Errors and lower-limits represent 1σ significance.

TABLE 2
 $\text{Ly}\alpha$ LUMINOSITY AND STAR FORMATION RATE FOR THE LAE CANDIDATES AT
 $z \approx 5.7$

No. ^a	$EW_0(\text{Ly}\alpha)^b$ (Å)	$L(\text{Ly}\alpha)^b$ (10^{42} ergs s $^{-1}$)	$SFR(\text{Ly}\alpha)^b$ (M_\odot yr $^{-1}$)	$L_{1270}^{b,c}$ (10^{28} ergs s $^{-1}$ Hz $^{-1}$)	$SFR(\text{UV})^b$ (M_\odot yr $^{-1}$)	$SFR(\text{Ly}\alpha)/SFR(\text{UV})^b$
1*	53 ± 31	9.2 ± 1.4	8.4 ± 1.3	8.7 ± 4.9	12.1 ± 6.8	0.69 ± 0.41
2*	46 ± 29	8.0 ± 1.6	7.3 ± 1.5	8.7 ± 5.1	12.1 ± 7.2	0.60 ± 0.38
3*	68 ± 60	8.2 ± 1.6	7.4 ± 1.5	6.0 ± 5.2	8.4 ± 7.2	0.89 ± 0.79
4*	67 ± 16	31.0 ± 1.6	28.2 ± 1.4	22.7 ± 5.2	31.8 ± 7.3	0.89 ± 0.21
5*	86 ± 74	10.7 ± 1.7	9.7 ± 1.6	6.1 ± 5.2	8.6 ± 7.3	1.14 ± 0.98
6*	> 74	8.1 ± 1.7	7.4 ± 1.6	< 5.4	< 7.5	> 0.98
7*	34 ± 16	7.9 ± 1.6	7.2 ± 1.4	11.5 ± 4.8	16.1 ± 6.8	0.45 ± 0.21
8*	20 ± 6	9.8 ± 1.7	9.0 ± 1.6	24.0 ± 5.5	33.6 ± 7.7	0.27 ± 0.08
9*	> 98	10.4 ± 1.7	9.4 ± 1.6	< 5.2	< 7.3	> 1.29
10*	22 ± 6	11.8 ± 1.8	10.8 ± 1.6	26.6 ± 5.8	37.2 ± 8.1	0.29 ± 0.08
11	25 ± 9	12.2 ± 2.2	11.1 ± 2.0	23.6 ± 7.2	33.1 ± 10.1	0.34 ± 0.12
12*	> 69	8.8 ± 1.9	8.0 ± 1.7	< 6.3	< 8.8	> 0.91
13*	> 175	18.4 ± 1.6	16.8 ± 1.5	< 5.2	< 7.3	> 2.30
14*	55 ± 16	21.2 ± 1.7	19.3 ± 1.5	19.0 ± 5.2	26.6 ± 7.3	0.72 ± 0.21
15*	19 ± 7	6.7 ± 1.6	6.1 ± 1.5	17.4 ± 4.9	24.3 ± 6.9	0.25 ± 0.09
16*	> 68	7.1 ± 1.7	6.4 ± 1.5	< 5.1	< 7.2	> 0.89
17*	35 ± 14	11.7 ± 2.0	10.6 ± 1.8	16.3 ± 6.0	22.8 ± 8.3	0.47 ± 0.19
18*	91 ± 57	19.1 ± 2.1	17.4 ± 1.9	10.3 ± 6.4	14.4 ± 8.9	1.20 ± 0.76
19*	77 ± 54	13.0 ± 1.7	11.9 ± 1.5	8.3 ± 5.7	11.7 ± 8.0	1.02 ± 0.71
20*	51 ± 36	8.0 ± 1.5	7.2 ± 1.4	7.7 ± 5.2	10.7 ± 7.2	0.68 ± 0.47
21*	> 79	8.4 ± 1.8	7.6 ± 1.6	< 5.2	< 7.3	> 1.04
22	> 74	12.8 ± 2.1	11.7 ± 1.9	< 8.5	< 11.9	> 0.98
23*	58 ± 35	10.1 ± 1.6	9.2 ± 1.5	8.6 ± 5.1	12.0 ± 7.1	0.76 ± 0.47
24*	> 100	12.3 ± 1.7	11.2 ± 1.6	< 6.1	< 8.5	> 1.32
25*	> 94	9.3 ± 1.4	8.5 ± 1.3	< 4.9	< 6.8	> 1.24
26*	> 71	6.5 ± 1.5	5.9 ± 1.3	< 4.5	< 6.4	> 0.93
27*	85 ± 36	16.3 ± 1.3	14.8 ± 1.1	9.4 ± 3.9	13.2 ± 5.4	1.12 ± 0.47
28*	> 77	7.6 ± 1.5	7.0 ± 1.4	< 4.9	< 6.8	> 1.02
29*	72 ± 49	11.1 ± 1.4	10.1 ± 1.3	7.6 ± 5.1	10.7 ± 7.1	0.95 ± 0.64
30*	66 ± 43	12.2 ± 1.7	11.1 ± 1.5	9.1 ± 5.7	12.7 ± 8.0	0.87 ± 0.56
31*	154 ± 114	20.3 ± 1.5	18.5 ± 1.4	6.5 ± 4.8	9.1 ± 6.7	2.03 ± 1.51
32	127 ± 112	18.5 ± 2.1	16.8 ± 2.0	7.2 ± 6.3	10.1 ± 8.8	1.67 ± 1.47
33*	30 ± 10	11.0 ± 1.8	10.0 ± 1.6	18.3 ± 5.3	25.6 ± 7.5	0.39 ± 0.13
34*	29 ± 13	7.3 ± 1.5	6.6 ± 1.3	12.6 ± 5.2	17.6 ± 7.3	0.38 ± 0.17
35*	42 ± 18	9.6 ± 1.3	8.7 ± 1.2	11.2 ± 4.5	15.7 ± 6.2	0.56 ± 0.24
36*	56 ± 36	9.4 ± 1.6	8.5 ± 1.5	8.3 ± 5.1	11.6 ± 7.2	0.74 ± 0.47
37*	> 100	12.4 ± 1.8	11.3 ± 1.6	< 6.1	< 8.6	> 1.31
38*	> 100	10.9 ± 1.7	9.9 ± 1.5	< 5.4	< 7.5	> 1.32
39*	89 ± 56	13.6 ± 1.4	12.3 ± 1.3	7.5 ± 4.7	10.5 ± 6.6	1.17 ± 0.74
40*	20 ± 4	13.3 ± 1.5	12.1 ± 1.4	32.3 ± 5.1	45.2 ± 7.1	0.27 ± 0.05
41*	> 103	11.2 ± 1.7	10.2 ± 1.5	< 5.3	< 7.5	> 1.36
42*	> 72	8.0 ± 1.6	7.3 ± 1.4	< 5.5	< 7.8	> 0.94
43*	91 ± 65	13.2 ± 1.5	12.0 ± 1.3	7.2 ± 5.1	10.0 ± 7.1	1.20 ± 0.86
44*	77 ± 51	11.6 ± 1.5	10.6 ± 1.4	7.4 ± 4.8	10.4 ± 6.7	1.02 ± 0.67
45*	55 ± 34	9.6 ± 1.5	8.8 ± 1.3	8.6 ± 5.0	12.0 ± 7.0	0.73 ± 0.44
46*	39 ± 11	16.7 ± 1.7	15.2 ± 1.6	20.9 ± 5.5	29.3 ± 7.7	0.52 ± 0.15
47*	42 ± 13	13.5 ± 1.3	12.3 ± 1.2	15.9 ± 4.6	22.3 ± 6.5	0.55 ± 0.17
48*	> 124	14.8 ± 1.8	13.5 ± 1.6	< 5.9	< 8.2	> 1.63
49*	> 84	8.0 ± 1.4	7.3 ± 1.2	< 4.7	< 6.6	> 1.11
50*	> 260	27.9 ± 1.6	25.4 ± 1.5	< 5.3	< 7.4	> 3.43
51*	> 88	9.5 ± 1.7	8.7 ± 1.5	< 5.3	< 7.4	> 1.16
52*	29 ± 10	10.7 ± 1.8	9.7 ± 1.6	18.4 ± 5.9	25.8 ± 8.2	0.38 ± 0.14
53*	53 ± 13	22.8 ± 1.5	20.7 ± 1.4	21.4 ± 4.9	30.0 ± 6.9	0.69 ± 0.17
54*	> 97	10.4 ± 1.7	9.5 ± 1.5	< 5.3	< 7.5	> 1.27
55*	> 97	9.8 ± 1.5	8.9 ± 1.3	< 5.0	< 7.0	> 1.28
56*	47 ± 29	8.2 ± 1.5	7.5 ± 1.4	8.6 ± 5.0	12.0 ± 7.1	0.62 ± 0.38
57*	51 ± 12	22.8 ± 1.6	20.8 ± 1.4	22.0 ± 5.1	30.8 ± 7.2	0.68 ± 0.16
58*	> 78	8.5 ± 1.7	7.8 ± 1.5	< 5.4	< 7.6	> 1.03
59*	68 ± 62	8.3 ± 1.5	7.6 ± 1.4	6.1 ± 5.4	8.5 ± 7.6	0.89 ± 0.81
60*	56 ± 26	13.7 ± 1.7	12.5 ± 1.5	12.1 ± 5.5	17.0 ± 7.6	0.73 ± 0.34
61*	15 ± 3	10.7 ± 1.5	9.7 ± 1.3	35.2 ± 4.8	49.3 ± 6.7	0.20 ± 0.04
62*	> 102	11.5 ± 1.7	10.5 ± 1.6	< 5.6	< 7.8	> 1.35
63*	48 ± 23	11.8 ± 1.6	10.8 ± 1.5	12.2 ± 5.5	17.1 ± 7.7	0.63 ± 0.30
64*	49 ± 25	9.4 ± 1.4	8.5 ± 1.3	9.5 ± 4.7	13.3 ± 6.6	0.64 ± 0.33
65*	68 ± 62	7.4 ± 1.4	6.7 ± 1.3	5.3 ± 4.7	7.5 ± 6.6	0.90 ± 0.81
66*	11 ± 3	7.1 ± 1.7	6.5 ± 1.5	31.5 ± 5.3	44.1 ± 7.5	0.15 ± 0.04
67*	15 ± 2	20.8 ± 1.8	18.9 ± 1.6	66.3 ± 6.3	92.9 ± 8.9	0.20 ± 0.03
68*	> 111	10.4 ± 1.4	9.4 ± 1.3	< 4.6	< 6.5	> 1.46
69*	> 101	10.0 ± 1.4	9.1 ± 1.3	< 4.9	< 6.8	> 1.33
70	> 89	12.6 ± 2.0	11.5 ± 1.8	< 7.0	< 9.8	> 1.17
71*	105 ± 34	31.1 ± 1.4	28.3 ± 1.3	14.6 ± 4.7	20.5 ± 6.6	1.38 ± 0.45

TABLE 2 — *Continued*

No. ^a	$EW_0(\text{Ly}\alpha)^b$ (\AA)	$L(\text{Ly}\alpha)^b$ (10^{42} ergs s $^{-1}$)	$SFR(\text{Ly}\alpha)^b$ (M_\odot yr $^{-1}$)	$L_{1270}^{b,c}$ (10^{28} ergs s $^{-1}$ Hz $^{-1}$)	$SFR(\text{UV})^b$ (M_\odot yr $^{-1}$)	$SFR(\text{Ly}\alpha)/SFR(\text{UV})^b$
72*	35 ± 25	6.5 ± 1.8	5.9 ± 1.6	9.2 ± 6.2	12.9 ± 8.7	0.46 ± 0.33
73*	73 ± 37	15.0 ± 1.5	13.7 ± 1.4	10.2 ± 5.1	14.2 ± 7.2	0.96 ± 0.49
74*	44 ± 23	9.9 ± 1.7	9.0 ± 1.6	11.1 ± 5.4	15.5 ± 7.6	0.58 ± 0.30
75*	90 ± 66	13.4 ± 1.6	12.2 ± 1.5	7.4 ± 5.3	10.3 ± 7.4	1.18 ± 0.87
76*	64 ± 27	14.8 ± 1.4	13.5 ± 1.3	11.5 ± 4.8	16.0 ± 6.7	0.84 ± 0.36
77*	53 ± 27	11.5 ± 1.6	10.5 ± 1.5	10.7 ± 5.3	15.0 ± 7.4	0.70 ± 0.36
78*	64 ± 17	23.8 ± 1.4	21.7 ± 1.3	18.4 ± 4.8	25.8 ± 6.8	0.84 ± 0.23
79*	79 ± 64	11.2 ± 1.9	10.2 ± 1.7	7.0 ± 5.5	9.8 ± 7.7	1.04 ± 0.84
80*	44 ± 21	10.6 ± 1.7	9.6 ± 1.5	11.8 ± 5.2	16.5 ± 7.2	0.58 ± 0.27
81*	> 76	8.9 ± 1.7	8.1 ± 1.6	< 5.7	< 8.0	> 1.00
82*	30 ± 15	7.7 ± 1.8	7.0 ± 1.6	12.7 ± 5.9	17.8 ± 8.3	0.39 ± 0.20
83*	31 ± 15	7.1 ± 1.6	6.5 ± 1.4	11.2 ± 4.9	15.7 ± 6.9	0.41 ± 0.20
84*	19 ± 3	18.1 ± 1.5	16.5 ± 1.4	47.5 ± 5.1	66.5 ± 7.1	0.25 ± 0.03
85*	27 ± 5	16.4 ± 1.8	14.9 ± 1.6	30.5 ± 5.3	42.7 ± 7.4	0.35 ± 0.07
86*	64 ± 63	7.7 ± 1.6	7.0 ± 1.5	5.9 ± 5.6	8.3 ± 7.9	0.84 ± 0.82
87*	46 ± 30	7.8 ± 1.6	7.1 ± 1.4	8.4 ± 5.2	11.7 ± 7.3	0.60 ± 0.39
88*	> 105	11.4 ± 1.7	10.4 ± 1.5	< 5.3	< 7.5	> 1.38
89*	> 92	10.8 ± 1.8	9.8 ± 1.6	< 5.8	< 8.1	> 1.22
90*	> 78	9.0 ± 1.7	8.2 ± 1.5	< 5.7	< 8.0	> 1.03
91*	> 89	9.9 ± 1.7	9.0 ± 1.5	< 5.5	< 7.7	> 1.17
92*	> 84	9.5 ± 1.8	8.7 ± 1.6	< 5.6	< 7.8	> 1.11
93*	> 79	8.8 ± 1.7	8.0 ± 1.5	< 5.5	< 7.7	> 1.05
94*	> 64	8.0 ± 1.7	7.3 ± 1.6	< 6.1	< 8.6	> 0.85
95*	> 79	8.5 ± 1.6	7.7 ± 1.5	< 5.3	< 7.4	> 1.05
96*	56 ± 25	13.5 ± 1.7	12.3 ± 1.5	11.8 ± 5.0	16.5 ± 7.0	0.74 ± 0.33
97*	46 ± 23	10.2 ± 1.6	9.3 ± 1.5	10.9 ± 5.1	15.3 ± 7.2	0.61 ± 0.30
98*	58 ± 26	14.8 ± 1.7	13.4 ± 1.6	12.6 ± 5.5	17.6 ± 7.7	0.76 ± 0.34
99*	64 ± 51	8.7 ± 1.5	7.9 ± 1.4	6.7 ± 5.2	9.4 ± 7.3	0.84 ± 0.67
100*	58 ± 58	7.1 ± 1.7	6.4 ± 1.6	6.0 ± 5.7	8.3 ± 8.0	0.77 ± 0.76
101*	> 98	10.2 ± 1.7	9.3 ± 1.5	< 5.1	< 7.2	> 1.29
102*	50 ± 41	7.6 ± 1.7	6.9 ± 1.6	7.4 ± 5.7	10.4 ± 8.0	0.66 ± 0.54
103	83 ± 63	11.2 ± 1.6	10.2 ± 1.5	6.7 ± 5.0	9.3 ± 6.9	1.09 ± 0.82
104	170 ± 128	22.3 ± 1.7	20.3 ± 1.5	6.5 ± 4.9	9.1 ± 6.8	2.24 ± 1.69
105*	> 59	6.5 ± 1.6	5.9 ± 1.5	< 5.4	< 7.6	> 0.78
106*	> 100	10.2 ± 1.6	9.3 ± 1.5	< 5.0	< 7.1	> 1.32
107*	> 92	10.1 ± 1.6	9.2 ± 1.4	< 5.4	< 7.6	> 1.21
108*	93 ± 69	13.4 ± 1.5	12.2 ± 1.4	7.1 ± 5.2	9.9 ± 7.2	1.23 ± 0.90
109*	37 ± 17	10.9 ± 2.0	9.9 ± 1.8	14.6 ± 6.1	20.4 ± 8.6	0.48 ± 0.22
110*	16 ± 5	8.4 ± 1.9	7.6 ± 1.7	25.1 ± 5.4	35.2 ± 7.6	0.22 ± 0.07
111*	17 ± 4	12.6 ± 1.9	11.5 ± 1.7	36.8 ± 6.1	51.5 ± 8.5	0.22 ± 0.05
112*	59 ± 48	8.8 ± 1.7	8.0 ± 1.6	7.4 ± 5.9	10.3 ± 8.2	0.78 ± 0.64
113*	> 92	10.5 ± 1.7	9.6 ± 1.5	< 5.6	< 7.9	> 1.21
114*	> 155	18.1 ± 1.8	16.5 ± 1.6	< 5.8	< 8.1	> 2.04
115*	45 ± 9	26.0 ± 1.7	23.6 ± 1.6	28.3 ± 5.1	39.6 ± 7.1	0.60 ± 0.11
116*	23 ± 11	6.3 ± 1.6	5.7 ± 1.5	13.8 ± 5.4	19.3 ± 7.6	0.30 ± 0.14
117	25 ± 10	11.4 ± 2.3	10.4 ± 2.1	22.9 ± 7.7	32.1 ± 10.8	0.32 ± 0.13
118*	94 ± 45	22.8 ± 1.7	20.7 ± 1.5	11.9 ± 5.7	16.7 ± 8.0	1.24 ± 0.60
119	25 ± 12	8.2 ± 2.0	7.5 ± 1.8	16.5 ± 6.9	23.1 ± 9.6	0.32 ± 0.16

^a Asterisks denote the statistical sample.

^b Errors and lower-limits represent 1σ significance.

^c The UV continuum luminosity at $\lambda = 1270$ \AA .

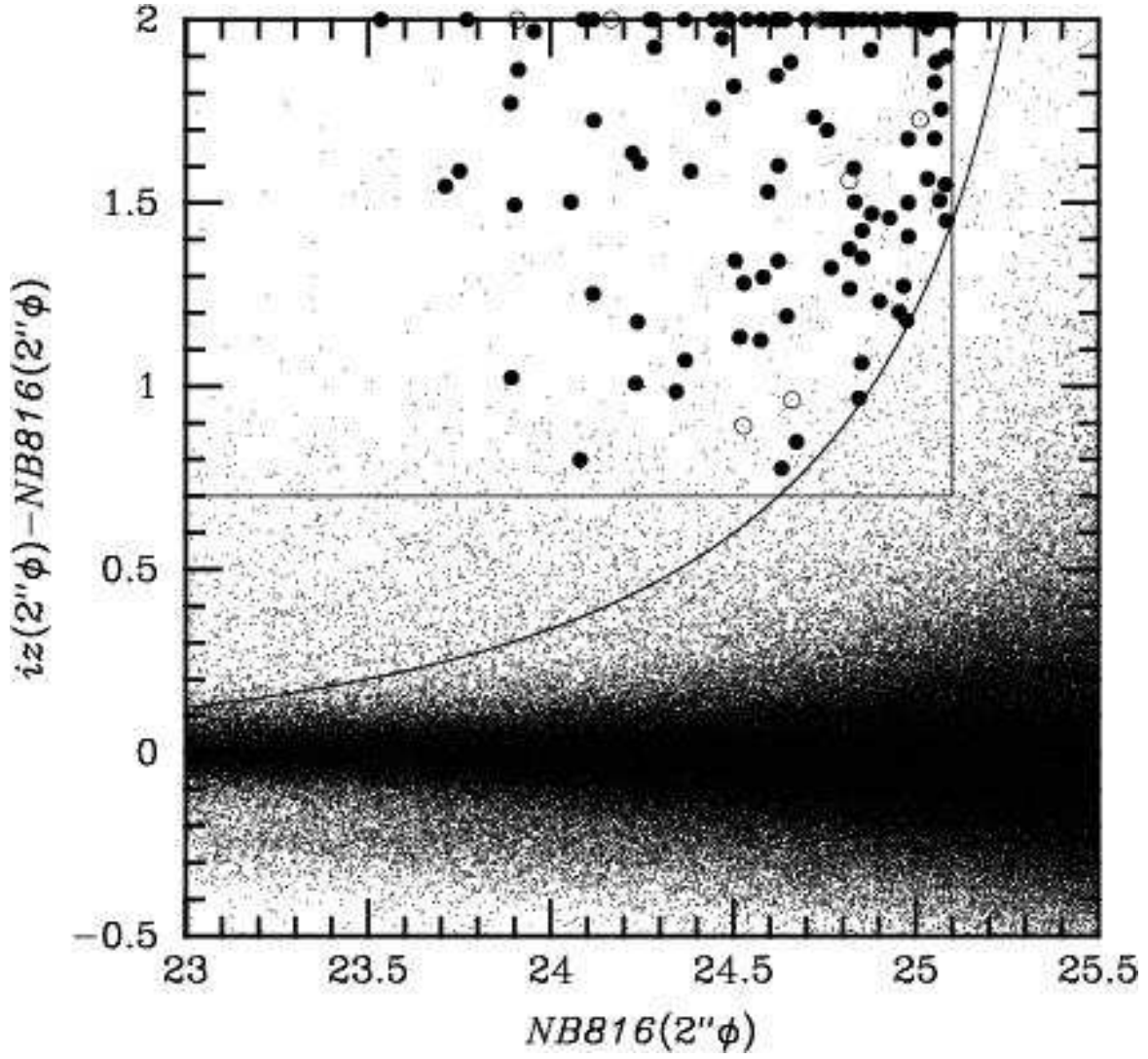


FIG. 1.— Diagram between $iz - NB816$ and $NB816$ for all objects detected with $NB816 < 26$. Our LAE candidates are shown by filled circles (the statistical sample) and open circles (the non-statistical sample). Objects with $iz - NB816 > 2$ are shown at $iz - NB816 = 2$ for clarity. The vertical line shows the detection limit of $NB816 = 25.1$. The horizontal line shows the selection criterion of $iz - NB816 = 0.7$. The curve shows the 3σ limit for the $iz - NB816$ color.

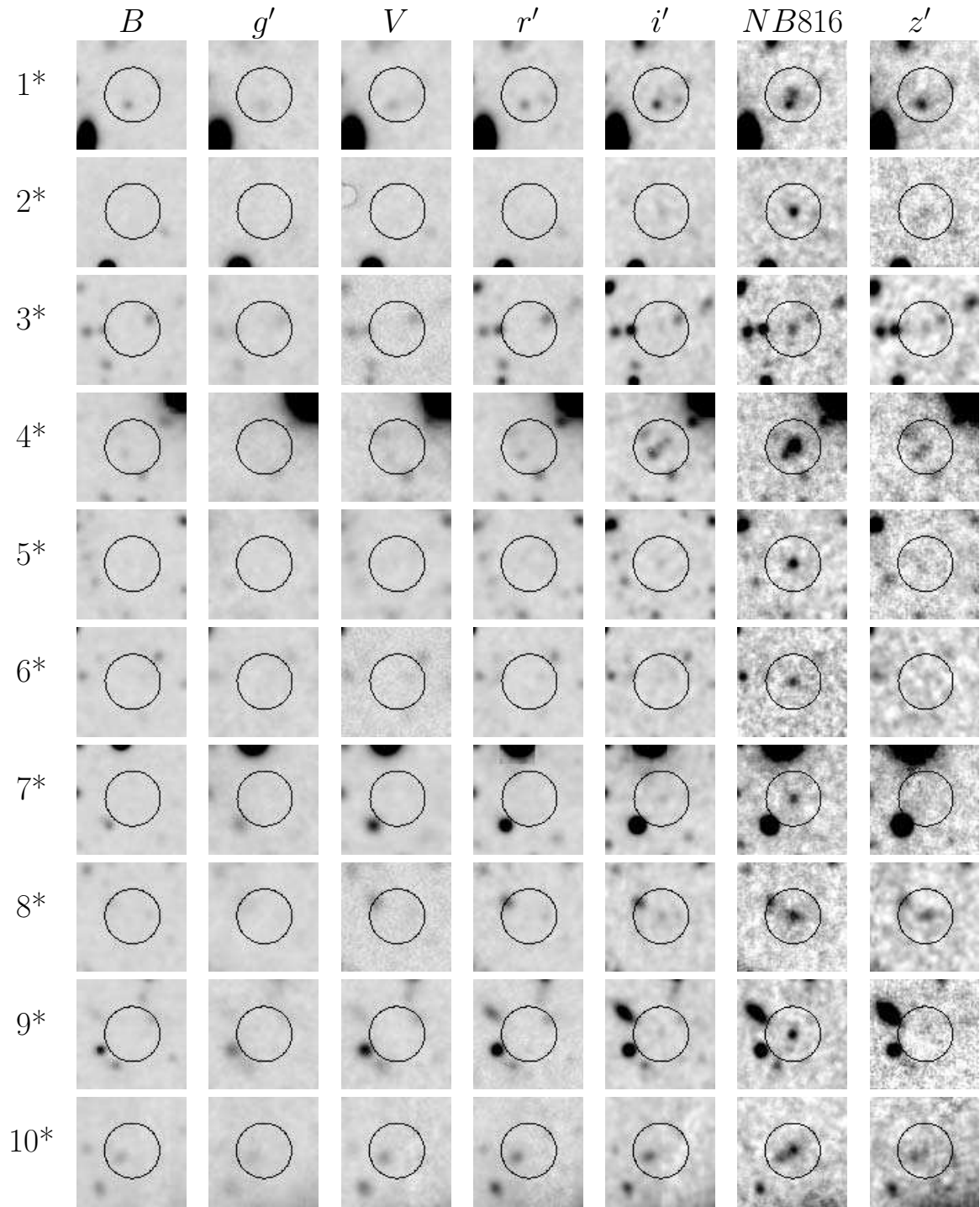


FIG. 2.— Broad-band and $NB816$ images of our LAE candidates at $z \approx 5.7$. Asterisks at the object number denote the statistical sample. Each box is $12''$ on a side (north is up and east is left). Each circle has $3''$ radius.

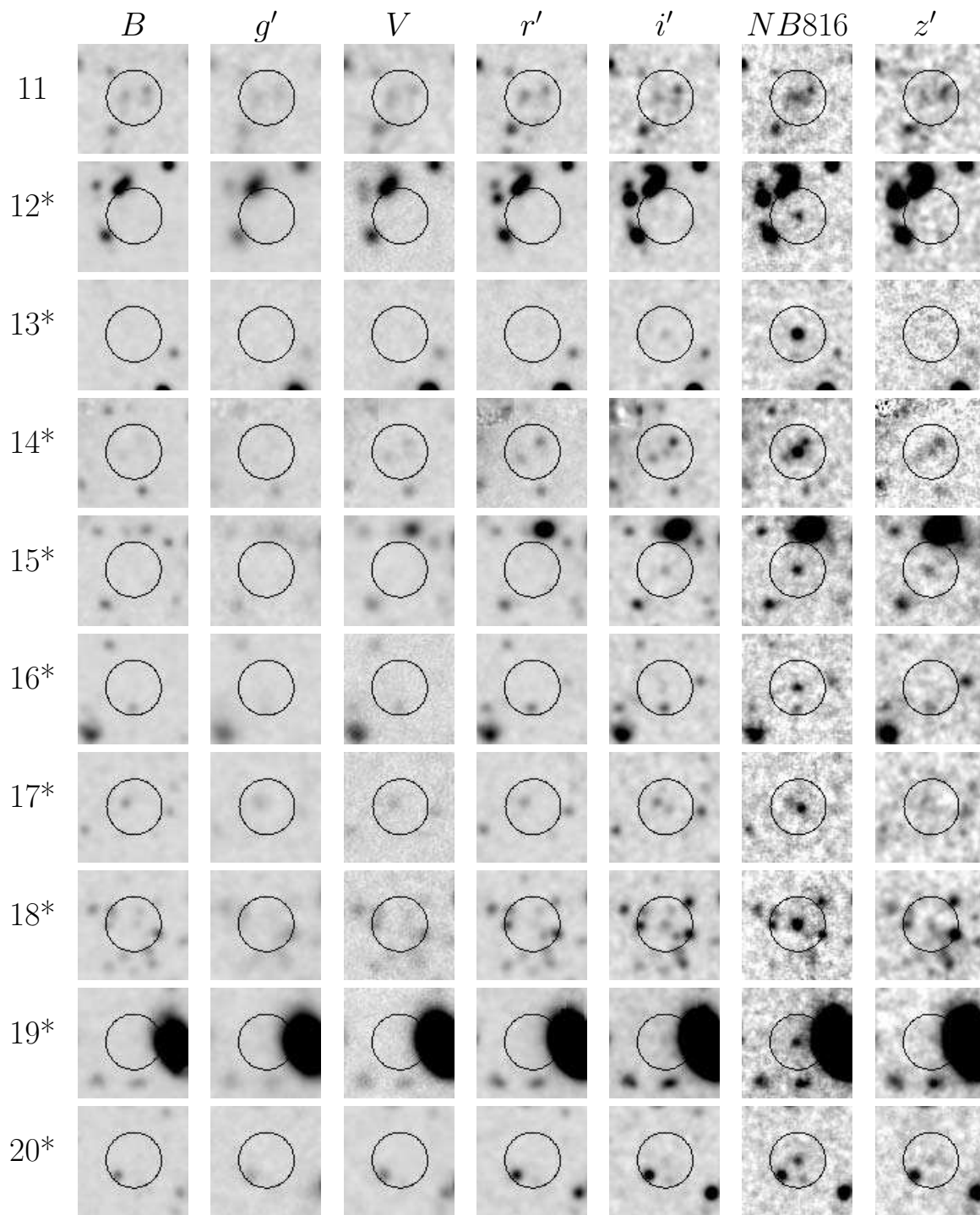


Fig. 2. — continued.

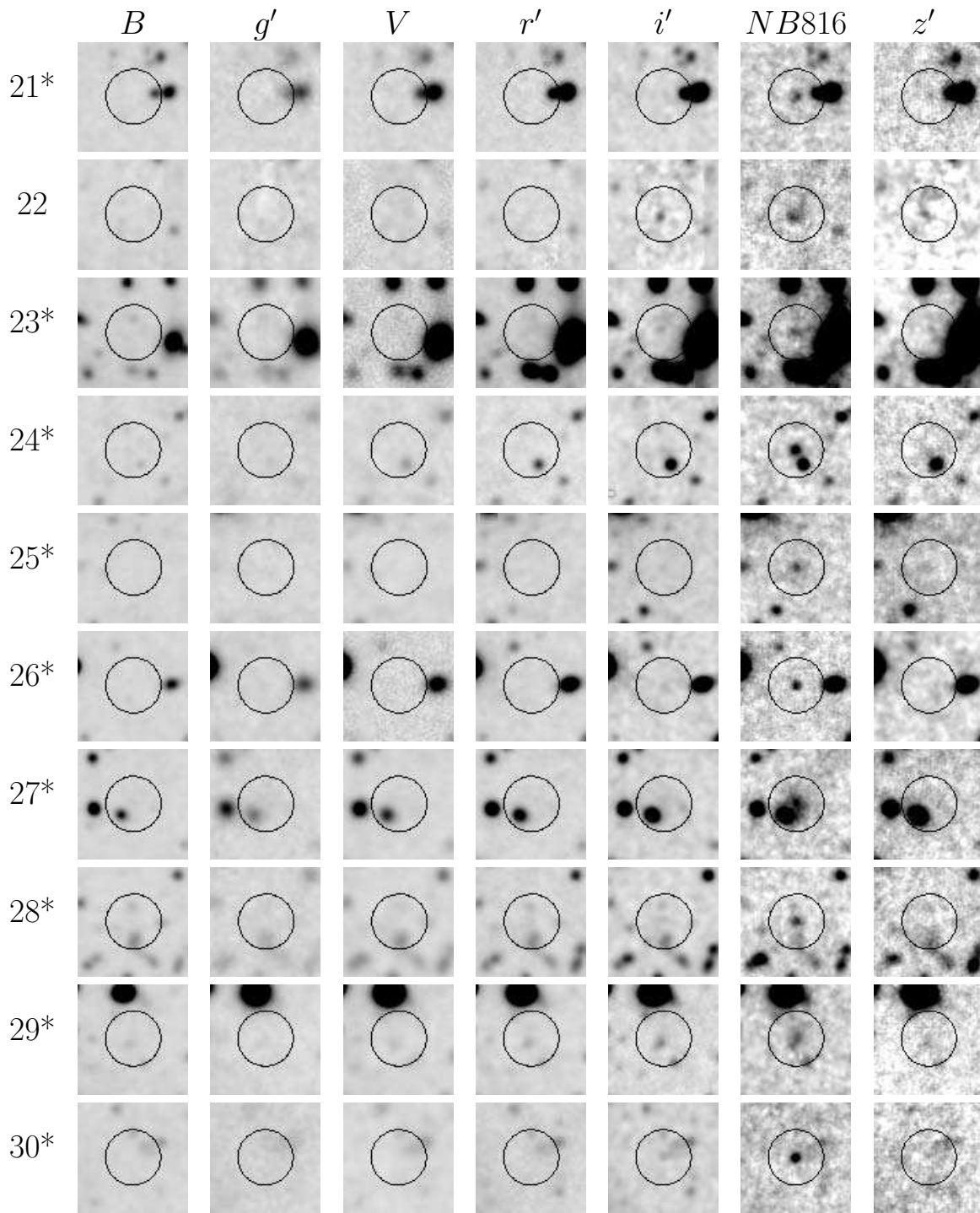


Fig. 2. — continued.

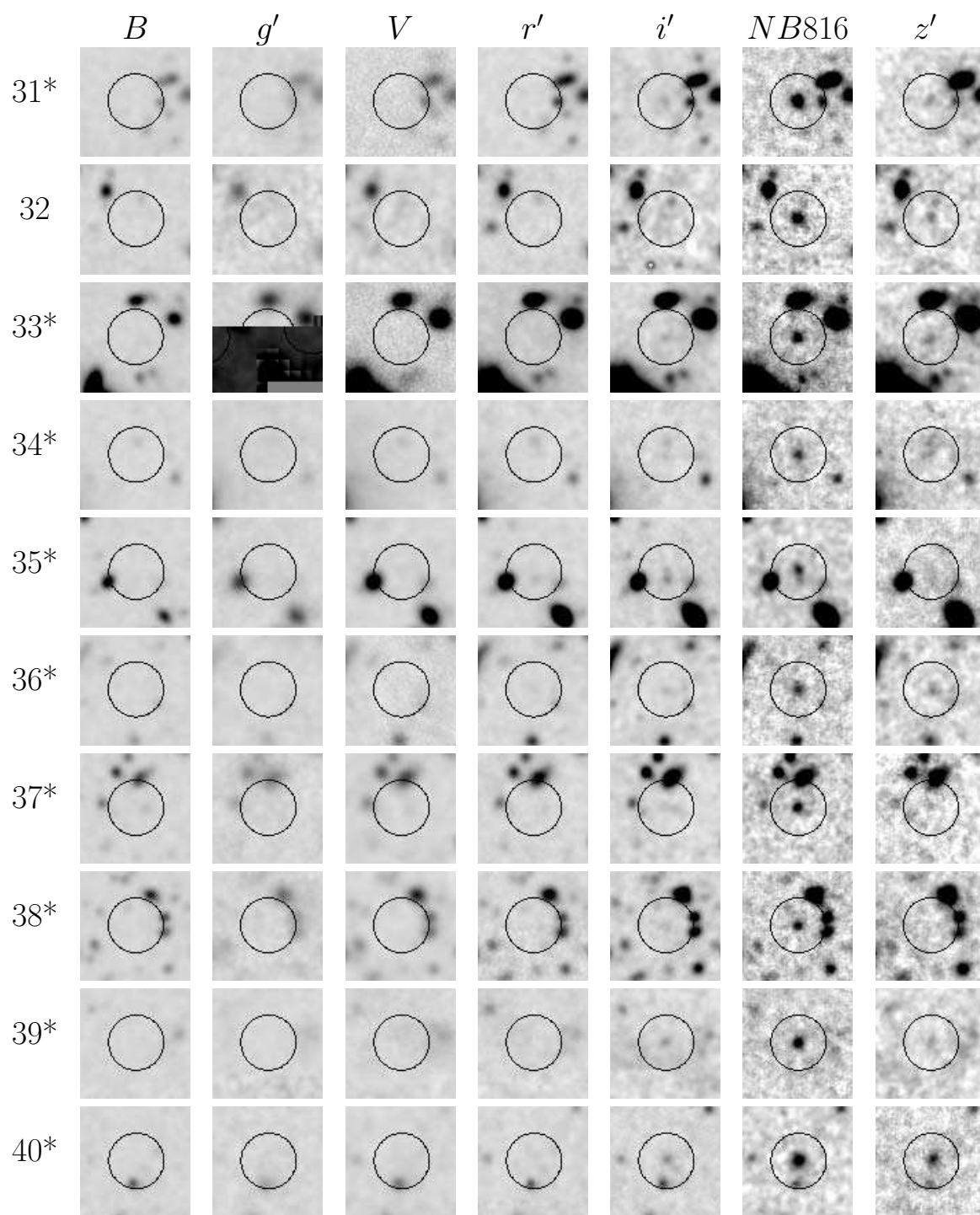


Fig. 2. — continued.

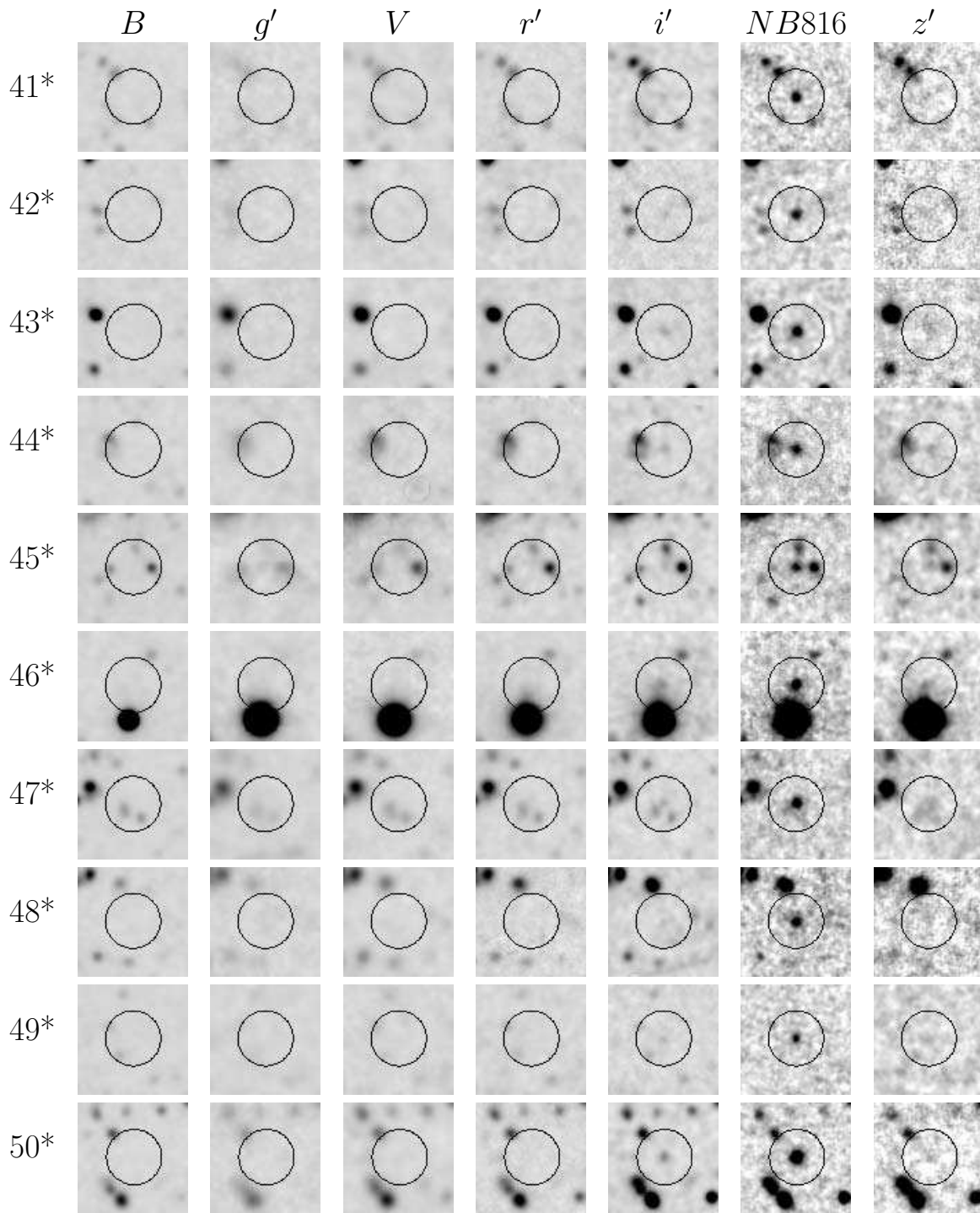


Fig. 2. — continued.

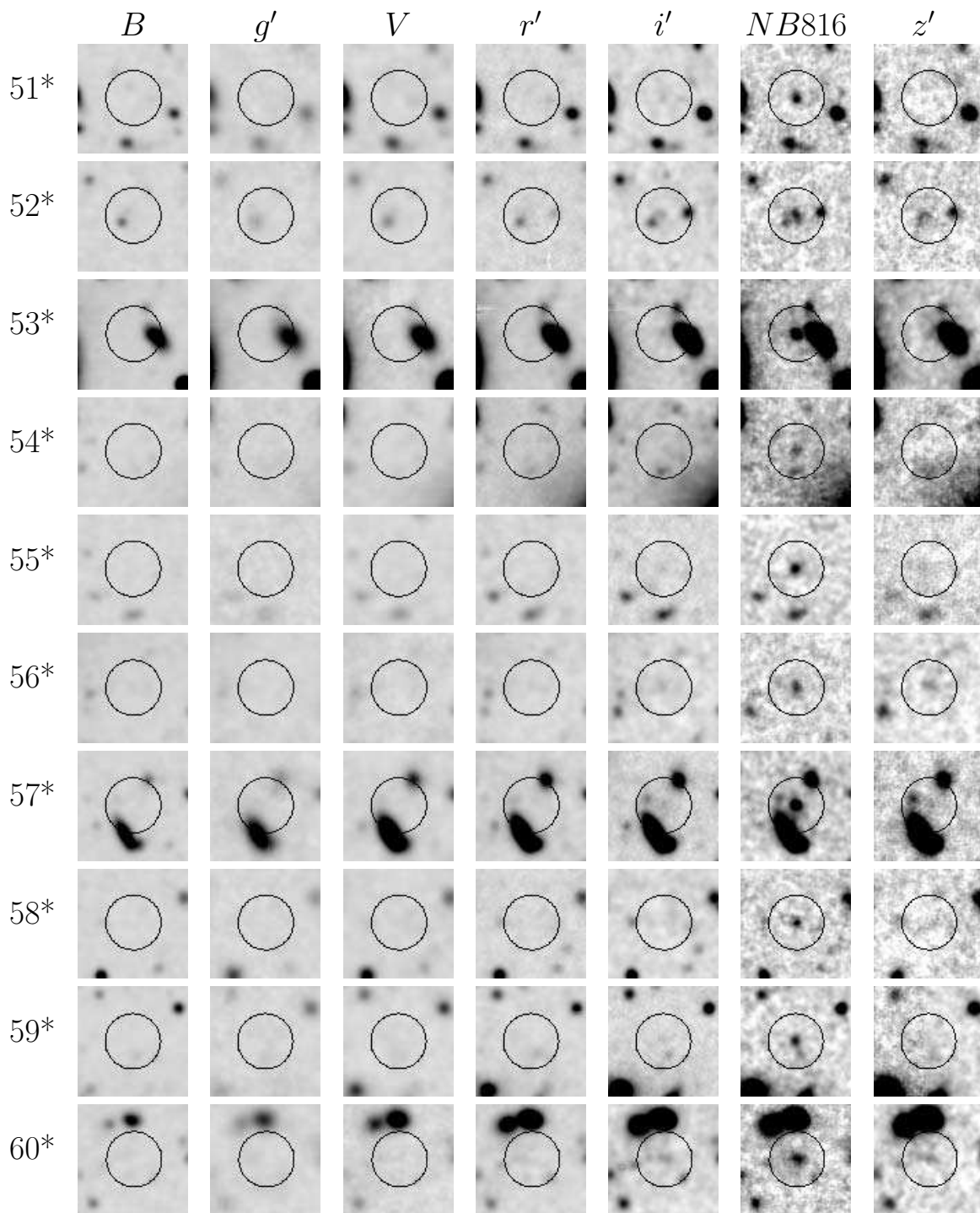


Fig. 2. — continued.

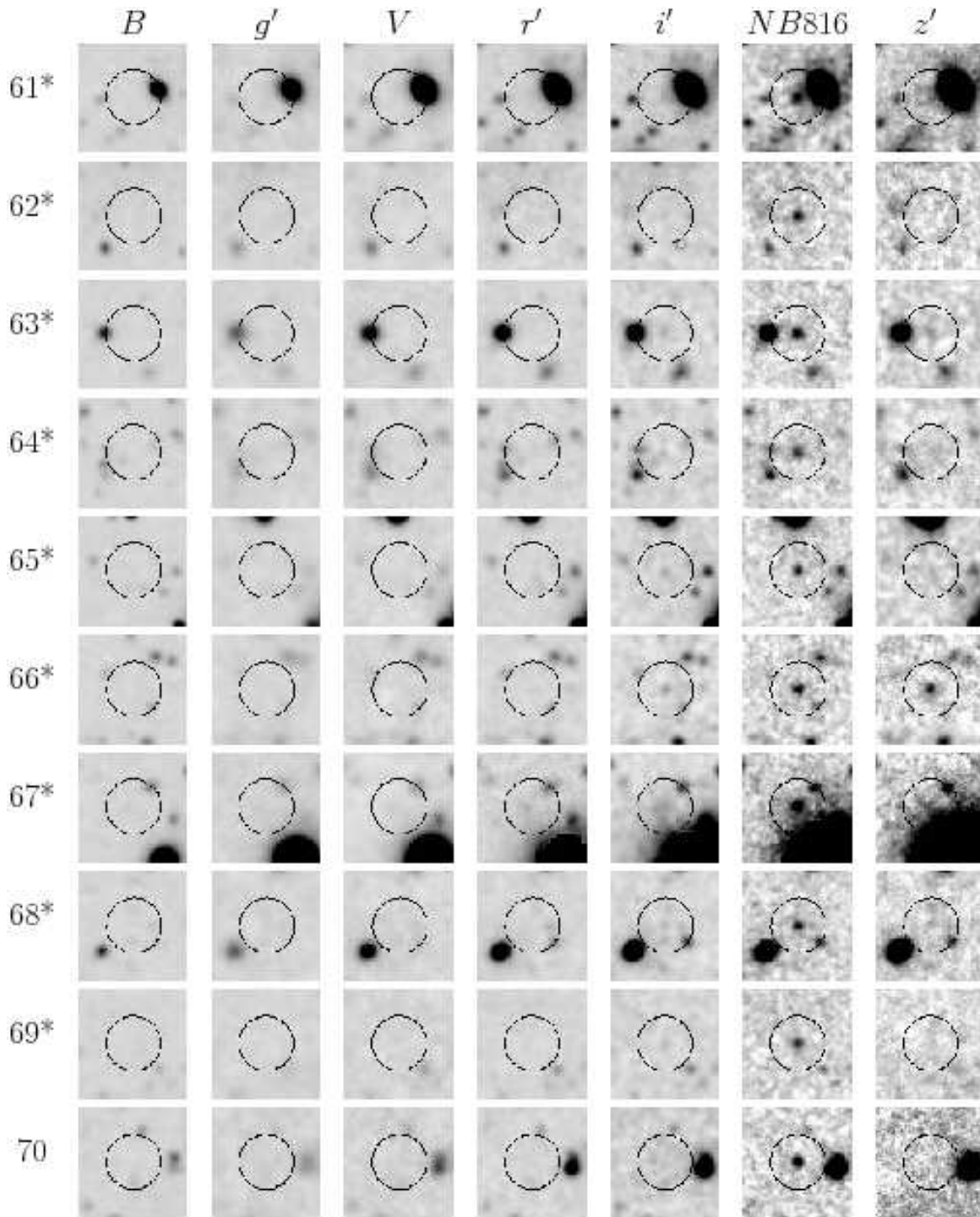


Fig. 2. — continued.

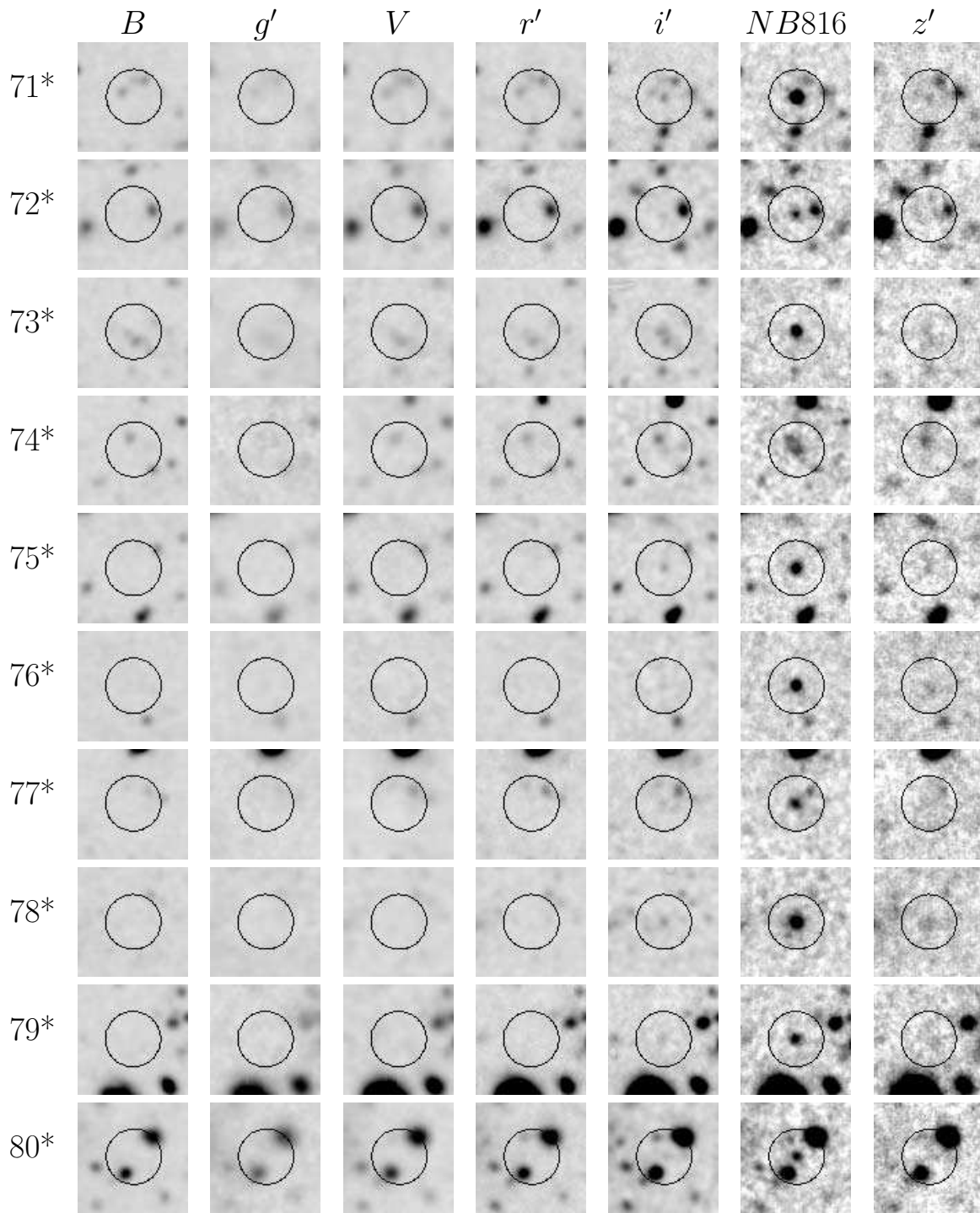


Fig. 2. — continued.

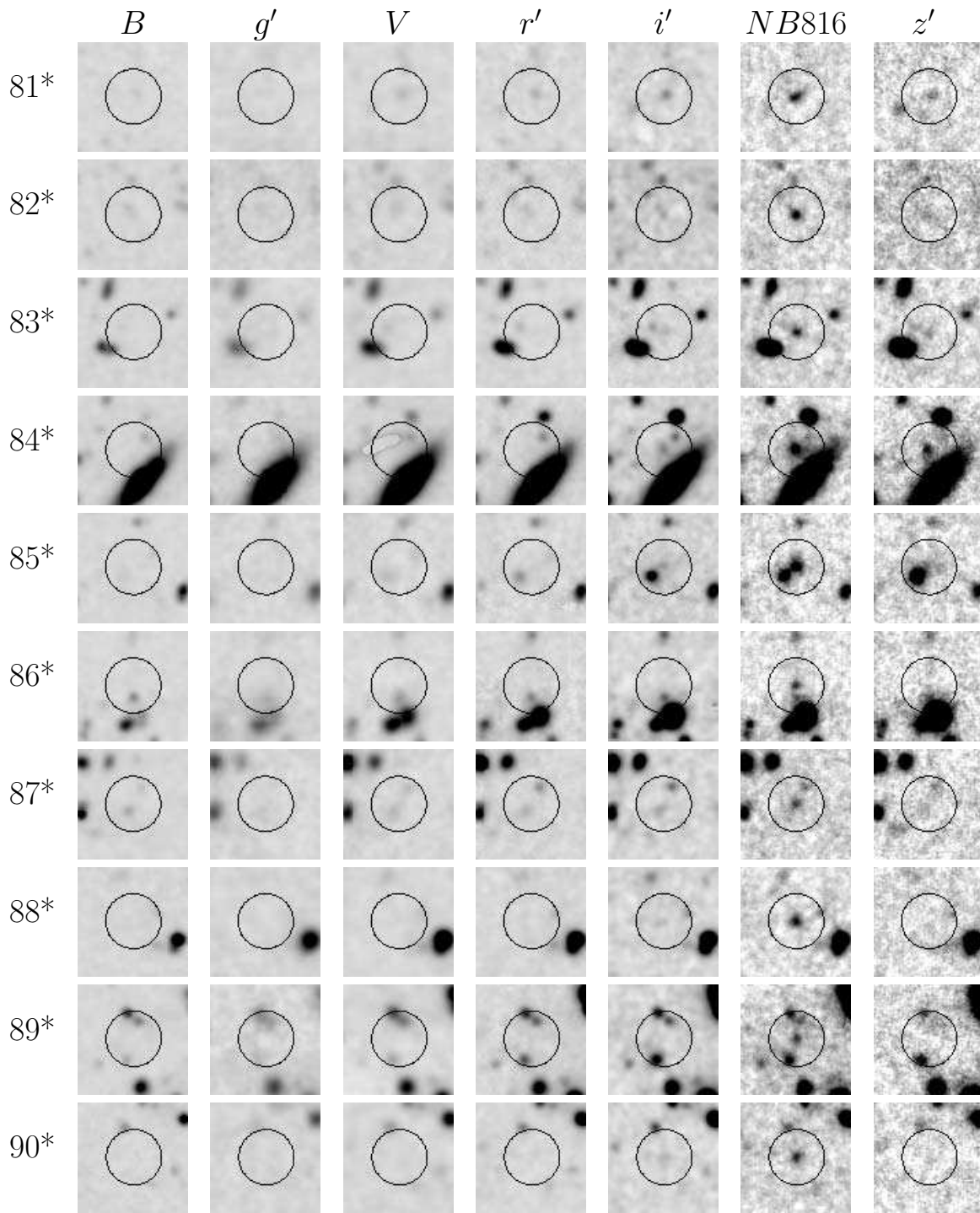


Fig. 2. — continued.

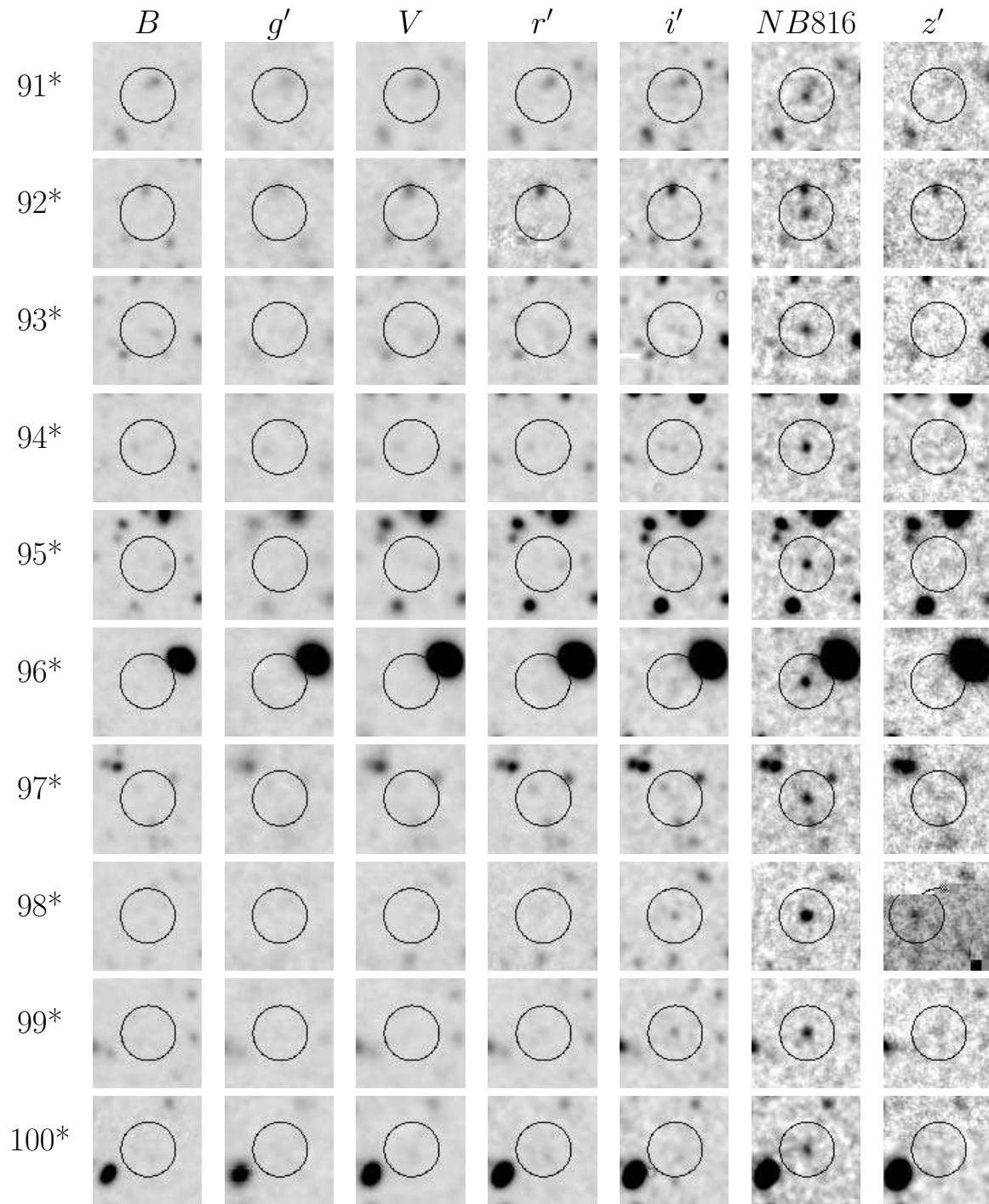


Fig. 2. — continued.

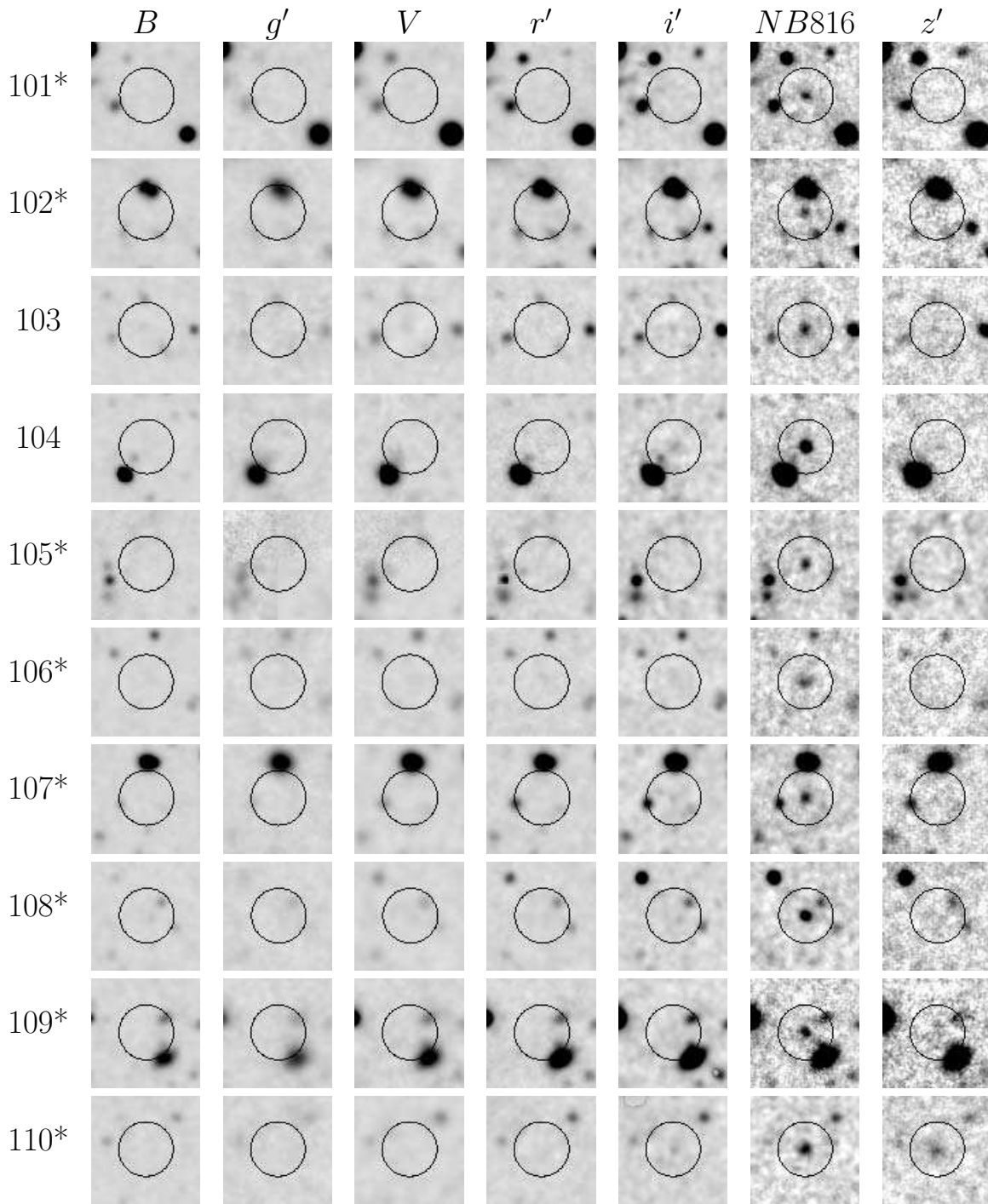


Fig. 2. — continued.

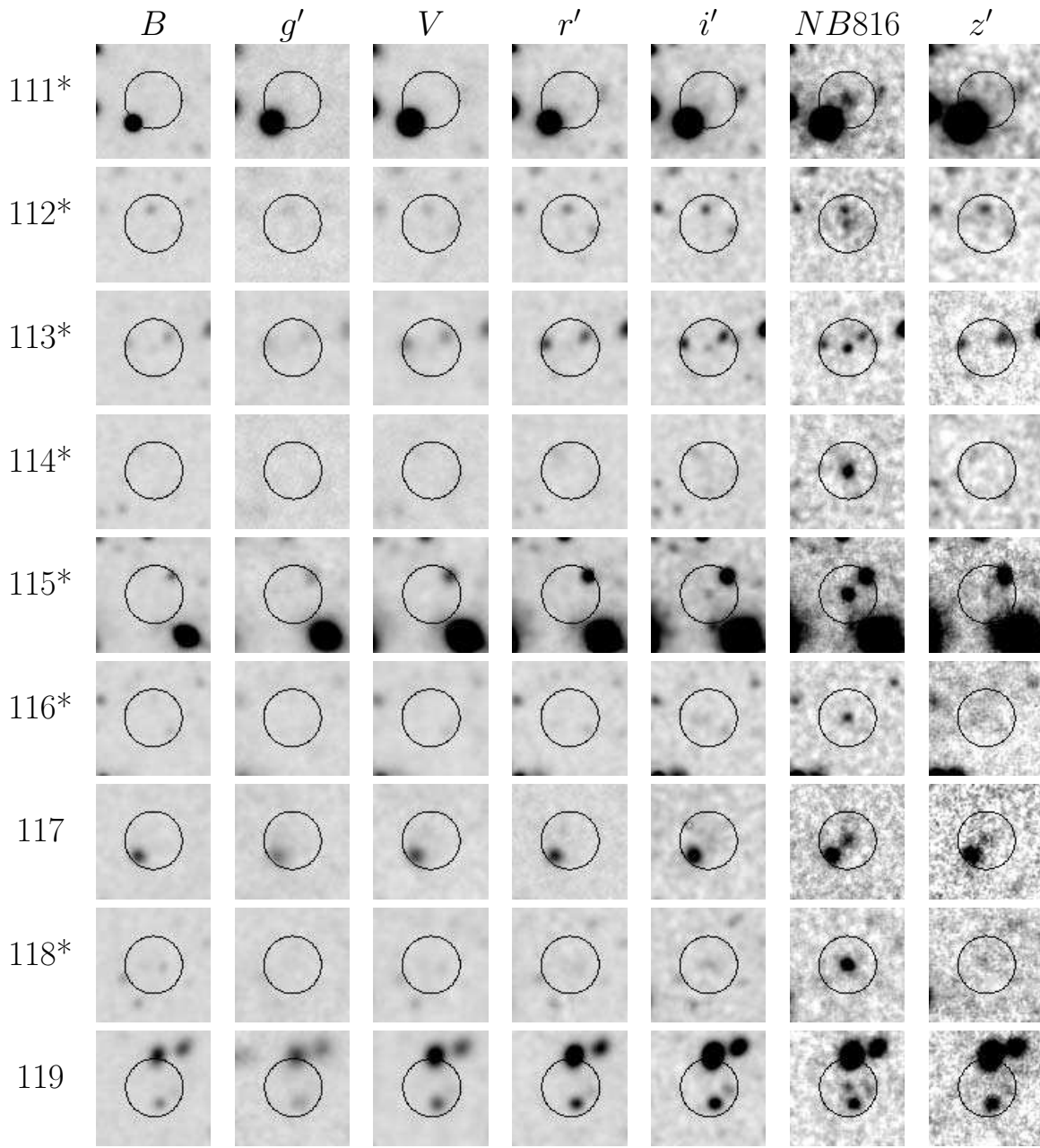


Fig. 2. — continued.

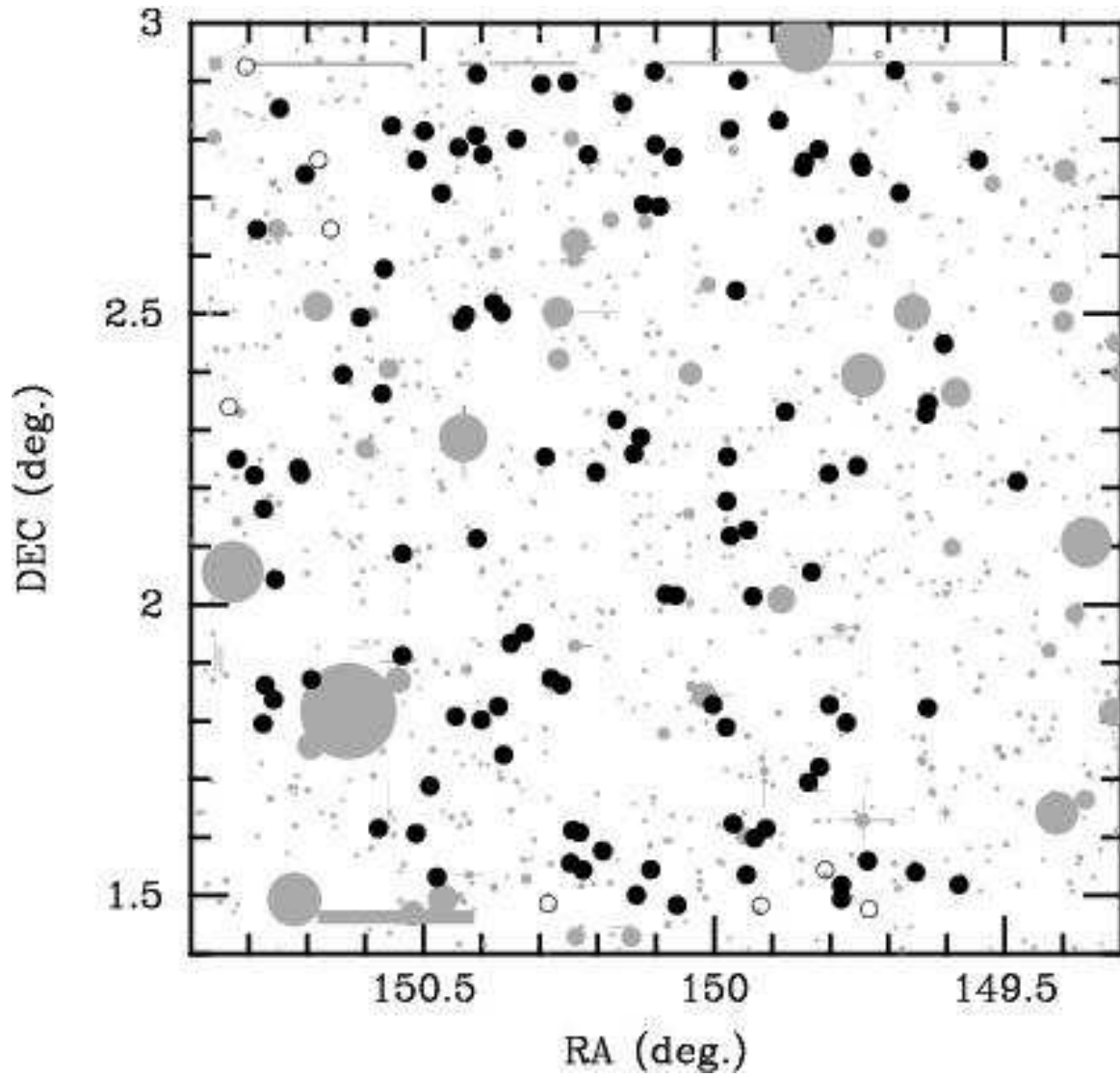


FIG. 3.— Spatial distributions of our 119 LAE candidates. The non-statistical sample is shown by open circles. The shadowed regions show the areas masked out for the detection.

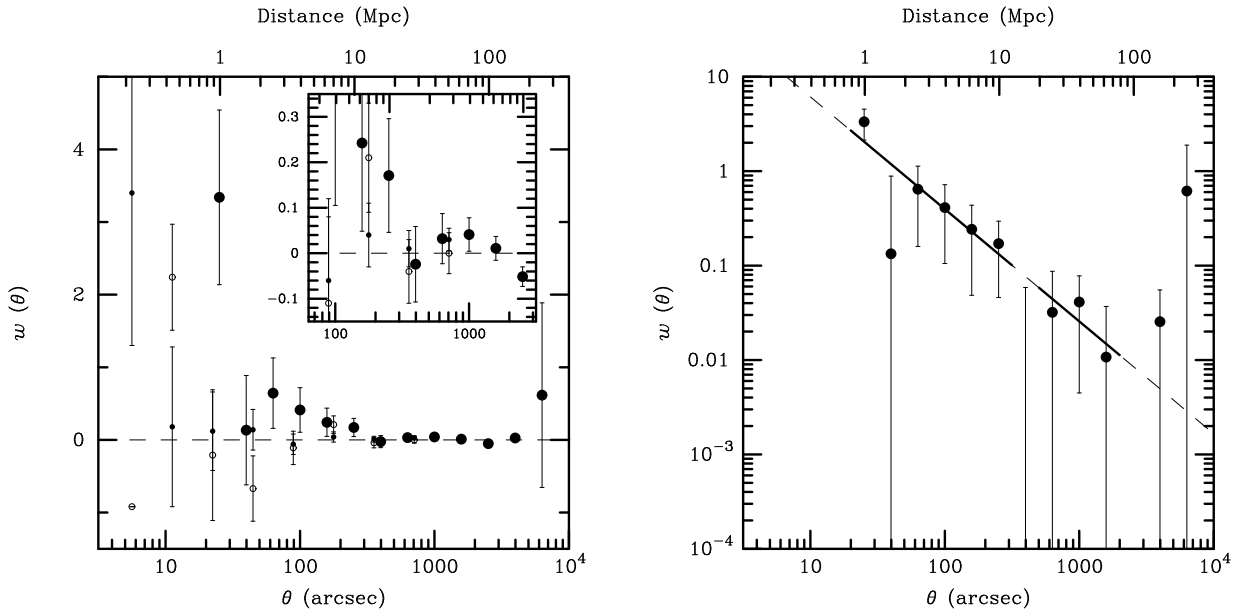


FIG. 4.— (left panel) Angular two-point correlation function of the 111 LAE candidates in the statistical sample (large filled circles). The small filled circles correspond to the the bright sample ($NB816 \leq 25.5$) of Shimasaku et al. (2006) while the open circles show the whole sample ($NB816 \leq 26.5$) of Shimasaku et al. (2006). Note that the $NB816$ limit of our LAE candidates is 25.1. The inset shows an expanded view at $60 \text{ arcsec} \leq \theta \leq 3000 \text{ arcsec}$. (right panel) The same as the left panel but $w(\theta)$ is shown by logarithmic scale. Large filled circles show the angular two-point correlation function by the 111 LAE candidates in the statistical sample. The dashed line shows the result of power-law fit of the data points at $25 \text{ arcsec} \leq \theta \leq 1585 \text{ arcsec}$ except the point at 398 arcsec (the fitting region is shown by the solid line).

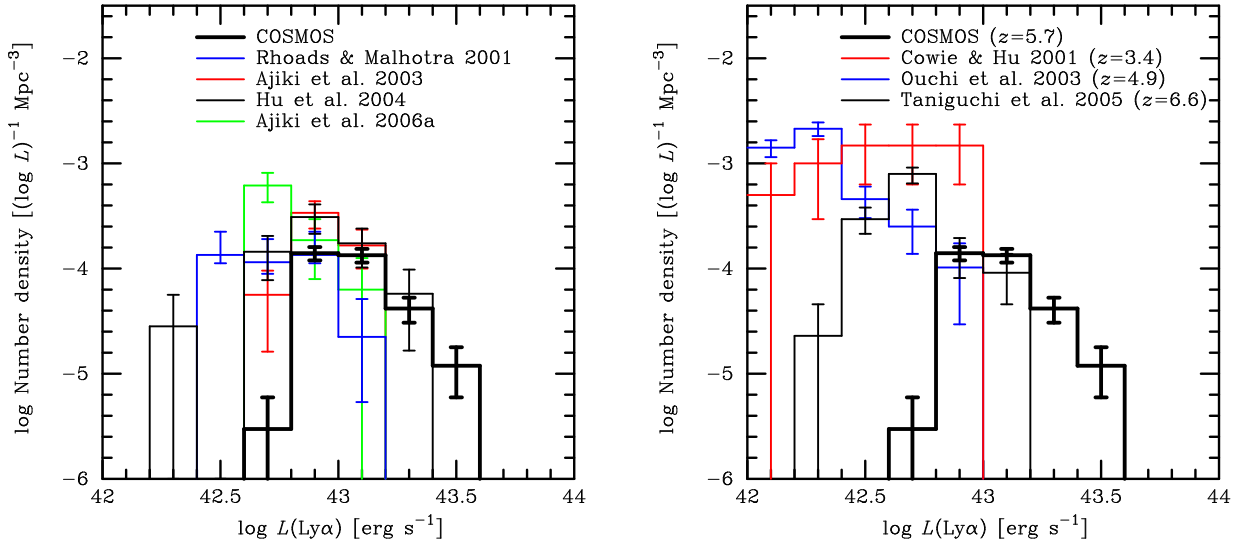


FIG. 5.— Ly α luminosity functions for our LAE candidates. (Left panel) Our result (thick line) is compared with those from previous surveys for LAEs at $z \sim 5.7$ (Rhoads & Malhotra 2001; Ajiki et al. 2003, 2006a; Hu et al. 2004). (Right panel) Our result (thick line) is compared with those from previous surveys for LAEs at $z = 3.4$ (Cowie & Hu 1998), $z = 4.9$ (Ouchi et al. 2003), and $z = 6.6$ (Taniguchi et al. 2005).

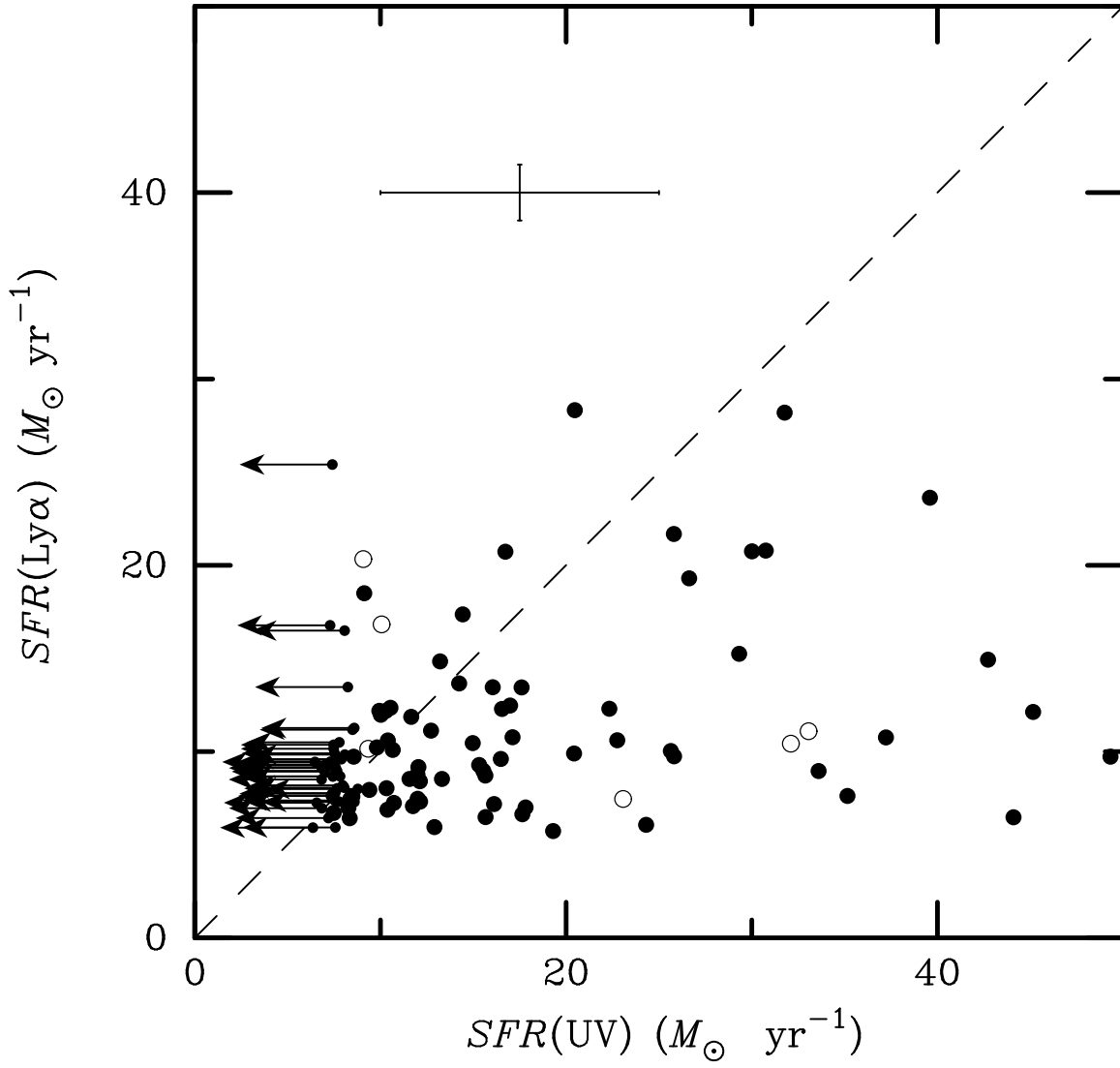


FIG. 6.— Comparison between $SFR(\text{Ly}\alpha)$ and $SFR(\text{UV})$ for our 119 LAE candidates. The non-statistical sample is shown by open circles. The dashed line shows the relation of $SFR(\text{Ly}\alpha)/SFR(\text{UV}) = 1$. The cross bar in upper left shows the typical 1σ error for our LAE candidates.